

Non-equilibrium view of the amorphous solidification of liquids with competing interactions

Cite as: J. Chem. Phys. **158**, 064506 (2023); <https://doi.org/10.1063/5.0132525>

Submitted: 28 October 2022 • Accepted: 22 January 2023 • Accepted Manuscript Online: 23 January 2023 • Published Online: 13 February 2023

 Ana Gabriela Carretas-Talamante,  Jesús Benigno Zepeda-López,  Edilio Lázaro-Lázaro, et al.



View Online



Export Citation



CrossMark

ARTICLES YOU MAY BE INTERESTED IN

[Structural relaxation, dynamical arrest, and aging in soft-sphere liquids](#)

The Journal of Chemical Physics **157**, 244504 (2022); <https://doi.org/10.1063/5.0121224>

[“Inner clocks” of glass-forming liquids](#)

The Journal of Chemical Physics **156**, 244506 (2022); <https://doi.org/10.1063/5.0087649>

[Computing chemical potentials of solutions from structure factors](#)

The Journal of Chemical Physics **157**, 121101 (2022); <https://doi.org/10.1063/5.0107059>

Learn More

The Journal
of Chemical Physics **Special Topics** Open for Submissions

Non-equilibrium view of the amorphous solidification of liquids with competing interactions

Cite as: J. Chem. Phys. 158, 064506 (2023); doi: 10.1063/5.0132525

Submitted: 28 October 2022 • Accepted: 22 January 2023 •

Published Online: 13 February 2023



View Online



Export Citation



CrossMark

Ana Gabriela Carretas-Talamante,¹  Jesús Benigno Zepeda-López,¹  Edilio Lázaro-Lázaro,¹ 
Luis Fernando Elizondo-Aguilera,²  and Magdaleno Medina-Noyola^{1,a)} 

AFFILIATIONS

¹Instituto de Física “Manuel Sandoval Vallarta,” Universidad Autónoma de San Luis Potosí, Álvaro Obregón 64, 78000 San Luis Potosí, Mexico

²Instituto de Física, Benemérita Universidad Autónoma de Puebla, Apartado Postal J-48 72570, Puebla, Mexico

Note: This paper is part of the JCP Special Topic on Colloidal Gels.

^{a)}Author to whom correspondence should be addressed: medina@ifisica.uaslp.mx

ABSTRACT

The interplay between short-range attractions and long-range repulsions (SALR) characterizes the so-called liquids with competing interactions, which are known to exhibit a variety of equilibrium and non-equilibrium phases. The theoretical description of the phenomenology associated with glassy or gel states in these systems has to take into account both the presence of thermodynamic instabilities (such as those defining the spinodal line and the so called λ line) and the limited capability to describe genuine non-equilibrium processes from first principles. Here, we report the first application of the non-equilibrium self-consistent generalized Langevin equation theory to the description of the dynamical arrest processes that occur in SALR systems after being instantaneously quenched into a state point in the regions of thermodynamic instability. The physical scenario predicted by this theory reveals an amazing interplay between the thermodynamically driven instabilities, favoring equilibrium macro- and micro-phase separation, and the kinetic arrest mechanisms, favoring non-equilibrium amorphous solidification of the liquid into an unexpected variety of glass and gel states.

Published under an exclusive license by AIP Publishing. <https://doi.org/10.1063/5.0132525>

I. INTRODUCTION

This work reports the first systematic application of the non-equilibrium self-consistent generalized Langevin equation theory^{1–3} to the description of non-equilibrium arrested states in fluids with competing short-range attractions and long-range repulsions (SALR).^{4,5} Such arrested states may prevent the fluid from reaching the experimentally elusive⁶ ordered phases expected at thermodynamic equilibrium conditions in the low-density low-temperature regime of these systems.⁷

As a context, let us first recall that van der Waals (vdW) molecular explanation of the gas–liquid coexistence had in mind a model fluid of spherical particles interacting by an excluded-volume repulsion plus a weaker short-ranged attraction.^{8,9} In choosing this simple model of a fluid, van der Waals was fortunate enough

since, for example, innocently adding a soft longer-ranged repulsive interaction immediately leads to a different class of systems, whose equilibrium phase behavior turns out to be far more complex. This more general class, characterized by the excluded-volume potential plus the competing SALR interactions, bears an enormous relevance in colloidal and soft materials. Familiar physical realizations of SALR conditions may be represented, for example, by the effective interaction between two charged particles (colloids, proteins, or macroions) in aqueous solution^{10,11} or between two colloids in colloid–polymer mixtures.¹²

Different approaches have been applied to determine the equilibrium phase diagram of SALR systems, including theoretical methods (integral equations,^{13–16} density functional theory,^{17–20} and field-theoretical models described by Ginzburg–Landau Hamiltonians^{21–23}) and Monte Carlo computer simulations.^{24–28}

As recently and thoroughly reviewed,^{4,7} the picture that emerges predicts a rich and diverse phenomenology, which includes the appearance at low densities of an equilibrium fluid phase of finite-sized clusters, the coexistence between disordered equilibrium (gas and liquid) phases and ordered (“modulated”) inhomogeneous phases, and the possibility that equilibrium microphase separation preempts the usual vdW gas–liquid coexistence.

These different phenomenological features correspond, in general, to different combinations of the short-range attraction and the long-range repulsion. A major challenge is, of course, to establish which salient features correspond to which regime in the four-dimensional parameter space spanned by the intensity and range of the two competing interactions. After careful analysis of experimental, simulation, and theoretical results, Liu and Xi⁴ suggested that most of SALR systems can be grouped in three different regimes, identified by the ratio between ranges of the attractive and repulsive interactions. They noticed that most model experimental SALR systems studied belong to a similar type, referred to as type I SALR systems, whereas many simulation works are type II SALR systems. As discussed in detail in Ref. 4, the difference between different types of SALR systems has strong impact on the final equilibrium phase diagram. As specified below, however, the present work will focus on still a third SALR regime, referred to in Ref. 4 as type III SALR systems.

Given this equilibrium scenario, the next most important issue is its actual experimental observability. This concern arises from the possible emergence of kinetic barriers to equilibration, which may lead to conditions of dynamic arrest, as suggested by early theoretical considerations^{16,29–31} and by molecular dynamics (MD) studies.^{32–37} The latter have confirmed, for example, the presence of a phase of stable, freely diffusing clusters of particles and of non-equilibrium phases of disordered arrested states. Beyond its fundamental relevance, this knowledge is important for many practical purposes, such as designing rules for the assembly of porous mesophases.³⁸ In contrast with Monte Carlo simulations, molecular dynamics [and Brownian dynamics (BD)] simulations mimic realistic trajectories in phase space, whose ensemble averages directly relate with the real dynamical phenomenology, actually observed since early and careful experimental studies.^{39–44}

Regarding the theoretical efforts to understand the formation of amorphous arrested states in SALR systems, let us mention the analysis aimed at determining if a glass transition exists in field-theoretical models. These efforts include the use of the replica approach^{21–23,45} and of the Langevin-equation version of these models.^{46,47} Early applications of mode coupling theory (MCT)^{48,49} to SALR systems were also reported by Grousson *et al.*⁴⁶ and by Geissler and Reichman,⁴⁷ although only for field-theoretical models.

However, developing a general fundamental microscopic theory of dynamical arrest in structural glasses, which explains the glass transition and extends the van der Waals picture to non-equilibrium conditions and to more complex interactions (such as SALR systems), has been the purpose of relevant work over the last half a century.⁵⁰ In this context, one should highlight the first-principles description of the dynamic properties of fluids near conditions of dynamic arrest provided by MCT,^{48,49} which predicts the location of the transition from equilibrium-fluid to dynamically arrested states. As early as in 2004, Wu *et al.*³¹ discussed the application of MCT

to the hard-sphere plus double Yukawa SALR type II interaction, predicting its fluid-to-glass transition diagram in the high-density high-temperature regime. Unfortunately, this work did not explore in detail the opposite (low-density low-temperature) regime.

Starting this exploration is precisely the purpose of the present work, motivated by the need to understand if the emergence of kinetic arrest and non-ergodicity might be the source of the experimental elusiveness of the predicted ordered (or “modulated”) equilibrium phases, which characterizes one specific SALR regime. In contrast with the work of Wu *et al.*, however, our work will not be based on MCT but on the more recent theory referred to as the self-consistent generalized Langevin equation (SCGLE) theory of colloid dynamics^{51–55} and dynamical arrest,^{56–58} which in most aspects is analogous to MCT.⁵⁹

In reality, however, the SCGLE theory, just like MCT, bears a fundamental constraint to equilibrium conditions, thus impeding the description of essential fingerprints of dynamic arrest, such as the aging of glass- and gel-forming liquids. The route of escape from this limitation, however, was provided in Ref. 60, which proposed a far-from-equilibrium extension of the Onsager theory of irreversible processes^{61,62} and the Onsager–Machlup theory of thermal fluctuations,^{63,64} leading to the general theory of irreversible processes in liquids, referred to as the non-equilibrium self-consistent generalized Langevin equation (NE-SCGLE) theory.¹ This more general approach contains as a particular case the original equilibrium SCGLE theory, which is thus enriched by the non-equilibrium kinetic perspective required to describe non-stationary processes.⁶⁵

Therefore, the present study will be based on the NE-SCGLE, a theory that has solidly demonstrated its ability to predict some of the most relevant universal signatures of both the glass and gel transitions, including aging effects, as well as very specific features reflecting the particular role of the molecular interactions involved in the explicit systems considered so far. For instance, for systems involving only excluded volume interactions, this theory accurately describes the process of formation of high-density hard-sphere-like glasses,^{2,3,66,67} whereas for liquids with excluded volume plus attractive interactions (i.e., those in vdW’s mind), it predicts the formation of sponge-like gels and porous glasses by arrested spinodal decomposition.^{68–71} Extended to multi-component systems,^{67,72} the NE-SCGLE theory opens the possibility of describing the aging of “double” and “single” glasses in mixtures of neutral^{57,73,74} and charged^{58,75} particles; the initial steps in this direction are highly encouraging.⁷⁴ Similarly, its extension to liquids formed by particles interacting by non-radially symmetric forces^{76–78} accurately predicts the non-equilibrium coupled translational and rotational dynamic arrest observed in simulations.⁷⁹

In this work, we start a systematic application of the theoretical infrastructure of the NE-SCGLE theory to the same model of SALR colloidal fluid studied by Wu *et al.*,³¹ namely, a three-dimensional fluid of hard spheres (HS) of diameter σ , interacting through a total pair potential $u(r) = u^{HS}(r) + u^{DY}(r)$, where $u^{HS}(r)$ is the hard-sphere potential and $u^{DY}(r)$ is the sum of two competing Yukawa interactions,

$$u^{DY}(r) = -\epsilon_1 \frac{\exp[-z_1(r/\sigma - 1)]}{r/\sigma} + \epsilon_2 \frac{\exp[-z_2(r/\sigma - 1)]}{r/\sigma}. \quad (1)$$

This model system will be referred to as the “hard-sphere plus double Yukawa” (HSDY) fluid, whose equilibrium phase diagram was outlined by Archer and collaborators^{17,18} using density functional theory within a random phase approximation for the free energy, an approximation also employed in this work.

In its simplest version, the NE-SCGLE theory is summarized by a set of equations describing the irreversible evolution of the non-equilibrium structural and dynamical properties of an instantaneously quenched glass-forming liquid. These properties include the non-equilibrium structure factor (NESF) $S(k; t)$ and the *collective* and *self*-intermediate scattering functions (NEISF) $F(k, \tau; t)$ and (self-NEISF) $F_S(k, \tau; t)$, from which the diffusion coefficient, relaxation times, and rheological properties can be derived. Each of these properties depend on the final density and temperature and on the waiting time t , after the quench, as well as on the various parameters characterizing the system (such as the interaction parameters $\epsilon_1, \epsilon_2, z_1$, and z_2). Thus, the analysis of this multidimensional dependence, in its various regimes, will require more than one detailed report and is completely out of the scope of the present work. Hence, here we shall only summarize the conceptual and practical infrastructure needed for such analysis and will illustrate its use focusing mostly on the structural properties, represented by the NESF $S(k; t)$ and by the corresponding non-equilibrium radial distribution function (NERDF) $g(r; t)$.

For clarity, in Sec. II, we summarize the relevant aspects of the NE-SCGLE theory and briefly explain the procedure for its application to this SALR model fluid. This includes introducing the mean field approximation of the free energy density functional, which determines the main features of the *equilibrium* structure and phase behavior of the system, and is also the fundamental thermodynamic input of the NE-SCGLE equations. Starting with Sec. III, we restrict ourselves to the particular regime of long-ranged repulsions ($z_1 \geq 1 > z_2$). This election of parameters will limit this work to exploring only type III SALR system,⁴ for which we will discuss what we refer to as the “glass transition diagram”; this is the NE-SCGLE complement of the concept of equilibrium phase diagram. In Sec. IV, we discuss the various density and temperature regimes of the behavior of the long- t asymptotic limit $S^a(k)$ of the NESF $S(k; t)$, whereas in Sec. V, this analysis is extended to the finite waiting-time regime to illustrate the predicted scenario of the aging of the structural properties. In Sec. VI, we summarize the main results of the present paper.

II. THE NE-SCGLE THEORY

The fundamental origin of the NE-SCGLE was laid down in detail in Refs. 1–3. However, a practical summary can be found in the supplementary material of Ref. 70, which highlights the main simplifying approximations leading to the version of this theory employed in this and in all its previous concrete applications. The present study will be a straightforward extension of the work reported in Refs. 68–71, which describes the predicted scenario of arrested spinodal decomposition in liquids with excluded-volume plus attractive interactions. The reader is invited to visit these references, which describe in all detail the conceptual and practical challenges found in applying the theory to quenches inside the spinodal region or inside other thermodynamically unstable regions of the state space. These references also illustrate the wealth of information provided

by the NE-SCGLE on the time-dependent physical properties of an attractive system under these non-equilibrium conditions. In particular, the novel concept of time-dependent non-equilibrium phase diagram that emerges from these applications is carefully explained in Ref. 71.

A. The NE-SCGLE equations

In its simplest version, the NE-SCGLE theory is summarized by a set of equations that describe the irreversible evolution of the non-equilibrium structural and dynamical properties of a model glass-forming liquid, formed by N identical spherical particles in a volume V that interact through a radially symmetric pair potential $u(r)$. It starts with the time evolution equation for the NESF $S(k; t) \equiv \overline{\delta n(\mathbf{k}; t) \delta n(-\mathbf{k}; t)}$, where the over-line indicates the average over a (non-equilibrium) statistical ensemble and where $\delta n(\mathbf{k}; t)$ is the Fourier transform of the fluctuations in the local particle number density $n(\mathbf{r}; t)$. For a system that is instantaneously quenched at time $t = 0$ from initial bulk density and temperature (n_i, T_i) to new final values (n, T) , constrained to remain spatially uniform ($\overline{n}(\mathbf{r}; t) = n \equiv N/V$), such an equation reads, for $t > 0$,

$$\frac{\partial S(k; t)}{\partial t} = -2k^2 D^0 b(t) n \mathcal{E}(k; n, T) [S(k; t) - 1/n \mathcal{E}(k; n, T)], \quad (2)$$

with D^0 being the short-time self-diffusion coefficient.⁸⁰

In this equation, the time-dependent mobility function $b(t)$ is defined as $b(t) \equiv D_L(t)/D^0$, with $D_L(t)$ being the long-time self-diffusion coefficient at evolution time t . This function couples the structural relaxation described by Eq. (2) with the non-equilibrium relaxation of the dynamic properties of the fluid. Such coupling is established by the following exact expression for $b(t)$:

$$b(t) = \left[1 + \int_0^\infty d\tau \Delta\zeta^*(\tau; t) \right]^{-1}, \quad (3)$$

in terms of the t -evolving, τ -dependent friction function $\Delta\zeta^*(\tau; t)$, for which the NE-SCGLE theory derives the following approximate expression:¹

$$\Delta\zeta^*(\tau; t) = \frac{D_0}{24\pi^3 n} \int d\mathbf{k} k^2 \left[\frac{S(k; t) - 1}{S(k; t)} \right]^2 F(k, \tau; t) F_S(k, \tau; t), \quad (4)$$

in terms of the NESF $S(k; t)$ and of the NEISF $F(k, \tau; t) \equiv N^{-1} \overline{\delta n(\mathbf{k}, t + \tau) \delta n(-\mathbf{k}, t)}$, where $\delta n(\mathbf{k}, t)$ is the FT of the thermal fluctuations $\delta n(\mathbf{r}, t) \equiv n(\mathbf{r}, t) - n$ of the local number density $n(\mathbf{r}, t)$ at time t . The self-NEISF $F_S(k, \tau; t)$ is defined as $F_S(k, \tau; t) \equiv \overline{\exp[i\mathbf{k} \cdot \Delta\mathbf{r}_T(t, \tau)]}$, with $\Delta\mathbf{r}_T(t, \tau) \equiv [\mathbf{r}_T(t + \tau) - \mathbf{r}_T(t)]$ being the displacement of one particle considered as a tracer. As before, the over-line indicates an average over a corresponding non-equilibrium statistical ensemble.

The previous equations are complemented by the memory-function equations for $F(k, \tau; t)$ and $F_S(k, \tau; t)$, written approximately, in terms of their Laplace transforms (LT) $F(k, z; t)$ and $F_S(k, z; t)$, as

$$F(k, z; t) = \frac{S(k; t)}{z + \frac{k^2 D^0 S^{-1}(k; t)}{1 + \lambda(k) \Delta\zeta^*(z; t)}} \quad (5)$$

and

$$F_S(k, z; t) = \frac{1}{z + \frac{k^2 D^0}{1 + \lambda(k) \Delta\zeta^*(z; t)}}, \quad (6)$$

where $\Delta\zeta^*(z; t)$ is the LT of $\Delta\zeta^*(\tau; t)$. In these equations $\lambda(k) \equiv 1/[1 + (k/k_c)^2]$ is an “interpolating function,”⁵⁶ with k_c being an empirically determined cutoff wave-vector. In the present work, we use $k_c = 1.305(2\pi)/\sigma$, with σ being the hard-core particle diameter of our HSDY model fluid, which guarantees that the hard-sphere liquid will have its dynamic arrest transition at a volume fraction $\phi_c = 0.582$, in agreement with simulations.⁶⁶

Equations (2)–(6) constitute the mathematical summary of the NE-SCGLE theory. Since the function $\mathcal{E}(k; n, T)$ is considered known, they constitute a closed system of equations for the time-dependent SF $S(k; t)$ and for the non-equilibrium dynamic properties $b(t)$, $\Delta\zeta^*(\tau; t)$, $F(k, \tau; t)$, and $F_S(k, \tau; t)$. Thus, Subsection II B defines the thermodynamic function $\mathcal{E}(k; n, T)$, explains its role in determining stability and structural properties.

B. Thermodynamic stability function $\mathcal{E}(k; n, T)$

The function $\mathcal{E}(k; n, T)$ is defined as the FT of $\mathcal{E}[r; n, T]$, which, in turn, is the second functional derivative of the Helmholtz free energy density-functional $\mathcal{F}[n, T]$,

$$\mathcal{E}[|\mathbf{r} - \mathbf{r}'|; n, T] \equiv \left(\frac{\delta^2 \mathcal{F}[n, T]/k_B T}{\delta n(\mathbf{r}) \delta n(\mathbf{r}')} \right), \quad (7)$$

evaluated at the uniform (bulk) density and temperature fields $n(\mathbf{r}, t) = n \equiv N/V$ and $T(\mathbf{r}, t) = T$. We refer to $\mathcal{E}(k; n, T)$ as the thermodynamic stability function, since it provides a criterion for the thermodynamic stability of the system. For example, the state function $\mathcal{E}(k; n, T)$, evaluated at $k = 0$, is related with the thermodynamic derivative $(\partial p/\partial n)_T$, where p is the pressure, as

$$\beta(\partial p/\partial n)_T = n\mathcal{E}(k = 0; n, T), \quad (8)$$

which is the so-called compressibility equation⁸⁴ ($\beta^{-1} \equiv k_B T$). As we see in Sec. II C, this equation of state allows us to determine the main features of the gas–liquid coexistence region, including the spinodal line, obtained from the condition $\mathcal{E}(k = 0; n, T) = 0$, which separates the state space (n, T) in the stable ($\mathcal{E}(k = 0; n, T) > 0$) and the unstable ($\mathcal{E}(k = 0; n, T) < 0$) equilibrium domains.

More generally, the function $\mathcal{E}(k; n, T)$ must be positive for all wave-vectors for the system to be stable, since if $\mathcal{E}(k; n, T) < 0$ for a finite k , the system would be unstable to density fluctuations of wavelength $2\pi/k$. Under some conditions, a domain $k^- \leq k \leq k^+$ may exist in which $\mathcal{E}(k; n, T) < 0$. Then, in analogy with the spinodal line, we define a λ line in the state space (n, T) by the threshold condition $k^- = k^+ = k_\lambda$, at which $\mathcal{E}(k_\lambda; n, T) = 0$.

The stability function $\mathcal{E}(k; n, T)$ also plays a relevant role in determining the structural properties of the system. For example, the equilibrium static structure factor (SF) $S^{eq}(k)$ is given by

$$S^{eq}(k) = 1/n\mathcal{E}(k; n, T), \quad (9)$$

which is just the well-known Ornstein–Zernike (OZ) equation,⁸⁴ as can be seen by writing $S^{eq}(k) = 1 + nh^{eq}(k)$ and $n\mathcal{E}(k; n, T) = 1 - nc(k)$, with $h^{eq}(k)$ being the FT of the equilibrium total correlation function (TCF) $h^{eq}(r)$ and $c(k)$ being the FT of the direct correlation function (DCF) $c(r)$. Clearly, the SF $S^{eq}(k)$ of a uniform system does not exist when $\mathcal{E}(k; n, T) < 0$.

From the kinetic perspective of Eq. (2), the OZ equation in Eq. (9) is just the equilibrium condition for the NESF $S(k; t)$. This is, in fact, the obvious stationary solution of the kinetic equation for $S(k; t)$ in Eq. (2), asymptotically attained at long times in the kinetic process of equilibration, i.e., $S(k; t \rightarrow \infty) = S^{eq}(k) = 1/n\mathcal{E}(k; n, T)$. However, under general non-equilibrium conditions, such as during the transient that follows an instantaneous quench, the NESF $S(k; t)$ is certainly NOT given by the OZ equation $S(k; t) = 1/n\mathcal{E}(k; n, T)$ but by the solution of Eq. (2), which provides a general manner to process the information contained in $\mathcal{E}(k; n, T)$ to determine $S(k; t)$. Thus, one can say that Eq. (2) is the non-equilibrium extension of the OZ equation. Note that as a thermodynamic input of this kinetic equation, negative values of $\mathcal{E}(k; n, T)$ are perfectly physical, leading, in fact, to some of the most remarkable predictions of the NE-SCGLE theory.

C. Mean field free energy functional $\mathcal{F}[n, T]$

In practice, we must identify a pertinent strategy to approximate $\mathcal{F}[n, T]$ for our three-dimensional HSDY model fluid. With the aim of adopting the same level of approximation as in the early theoretical discussions of the equilibrium phase diagram of SALR systems, we follow Refs. 13, 17, and 18 in writing $\mathcal{F}[n, T]$ as the sum $\mathcal{F}[n, T] = \mathcal{F}^{HS}[n, T] + \mathcal{F}^{DY}[n, T]$ of the exact hard-sphere free energy $\mathcal{F}^{HS}[n, T]$ plus the contribution $\mathcal{F}^{DY}[n, T]$ of the double Yukawa. A simple explicit expression for the latter is provided by its random phase approximation (RPA), within which $\mathcal{F}[n, T]$ is given by

$$\mathcal{F}[n, T] = \mathcal{F}^{HS}[n, T] + \frac{1}{2} \int d\mathbf{r} \int d\mathbf{r}' n(\mathbf{r}) u^{DY}(|\mathbf{r} - \mathbf{r}'|) n(\mathbf{r}'), \quad (10)$$

and the function $\mathcal{E}[|\mathbf{r} - \mathbf{r}'|; n, T]$ of Eq. (7) is given by

$$\mathcal{E}[|\mathbf{r} - \mathbf{r}'|; n, T] = \mathcal{E}^{HS}[|\mathbf{r} - \mathbf{r}'|; \phi] + \beta u^{DY}(|\mathbf{r} - \mathbf{r}'|), \quad (11)$$

whose FT reads

$$\mathcal{E}(k; n, T) = \mathcal{E}^{HS}(k; \phi) + \beta u^{DY}(k). \quad (12)$$

Writing $\mathcal{F}^{HS}[n, T]$ as $\mathcal{F}^{HS}[n, T] = \mathcal{F}^{HS}_{id}[n, T] + \mathcal{F}^{HS}_{ex}[n, T]$, where $\mathcal{F}^{HS}_{id}[n, T]$ is the ideal-gas value and $\mathcal{F}^{HS}_{ex}[n, T]$ is the “excess” HS contribution,⁸⁵ allows us to write Eq. (7) for the pure HS system as

$$\mathcal{E}^{HS}[|\mathbf{r} - \mathbf{r}'|; n, T] = \delta(\mathbf{r} - \mathbf{r}')/n - c^{HS}(|\mathbf{r} - \mathbf{r}'|; n, T) \quad (13)$$

with $c^{HS}(|\mathbf{r} - \mathbf{r}'|; n, T)$, defined by $c^{HS}(|\mathbf{r} - \mathbf{r}'|; n, T) \equiv -\beta(\delta^2 \mathcal{F}^{HS}_{ex}[n, T]/\delta n(\mathbf{r}) \delta n(\mathbf{r}'))$, being the exact HS DCF. In Fourier space, this equation reads $\mathcal{E}^{HS}(k; \phi) = 1/n - c^{HS}(k; \phi)$. As

in Refs. 17 and 18, here we will also approximate $c^{HS}(k; \phi)$ by its Percus–Yevick (PY) approximation⁸⁶ but complemented with its Verlet–Weis (VW) correction,⁸⁷ $c^{HS}(k; \phi) \approx c_{PYVW}^{HS}(k; \phi)$. Thus, the approximate thermodynamic input $\mathcal{E}(k; n, T)$ that we shall employ in this work is finally written as

$$\mathcal{E}(k; n, T) \approx 1/n - c_{PYVW}^{HS}(k; \phi) + \beta u^{DY}(k). \quad (14)$$

D. Equilibrium properties of the HSDY model

We may now use this approximate expression for the thermodynamic input $\mathcal{E}(k; n, T)$ of the NE-SCGLE equations, Eqs. (2)–(6), whose solution will describe the non-equilibrium response of the liquid after the instantaneous quench. For reference, however, let us first summarize some purely equilibrium properties that directly derive from the RPA for the thermodynamic input $\mathcal{E}(k; n, T)$ in Eq. (14), applied to the HSDY potential. For this, let us rewrite the DY term in Eq. (1) in dimensionless form as

$$\beta u^{DY}(r) = -\epsilon \frac{\exp[-z_1(r/\sigma - 1)]}{r/\sigma} + A \frac{\exp[-z_2(r/\sigma - 1)]}{r/\sigma}, \quad (15)$$

with $\epsilon \equiv \epsilon_1/k_B T$ and $A \equiv \epsilon_2/k_B T$.

Following Refs. 17 and 18, we have in mind a colloid–polymer mixture and consider the (“athermal”) conditions in which the physical temperature T is kept fixed and the strength of the attraction is controlled by varying the polymer concentration, i.e., ϵ^{-1} plays the role of an effective temperature $T_{eff} = \epsilon^{-1}$, which for simplicity in notation will be denoted as T . Thus, if the particle charge and ionic strength can be assumed fixed, we can treat the parameters A and z_2 (the intensity and range of the electrostatic repulsion) as fixed parameters. As a result, the function $\mathcal{E}(k; n, T)$ will actually depend on the dimensionless concentration $n^* \equiv n\sigma^3$, which we shall continue denoting by n (or in terms of the packing fraction $\phi = \pi n/6$), and on the effective temperature T . This dependence is additional to the dependence of $\mathcal{E}(k; \phi, T)$ on the potential parameters A , z_1 , and z_2 .

E. Equilibrium structure of the HSDY model

The first relevant property to discuss is, of course, the SF $S^{eq}(k; n, T)$ given by Eq. (9), which for notational convenience

we will denote as $S(k; n, T)$. From now on, we will consider a HSDY fluid with fixed parameters $z_1 = 1$, $z_2 = 0.5$, and $A = 0.5$, which, according to Ref. 4, corresponds to a type III SALR system. Figure 1(a) exhibits the main distinctive feature of the SF, previously discussed by Sear and Gelbart¹³ and by Archer *et al.*¹⁷ for the same HSDY model within the RPA. We refer to the development of a large peak centered at a small but finite wave vector $k = k_\lambda$ (referred to as the “cluster” peak¹⁷). This peak is associated with the propensity to the spontaneous formation of clusters in the equilibrium fluid, with its height $S(k_\lambda; \phi, T)$ increasing and its position k_λ decreasing, as the temperature T is reduced along a given isochore ($\phi = 0.15$, in the present case).

According to the RPA results in Fig. 1(a), $S(k_\lambda; \phi, T)$ actually diverges as the temperature T reaches a singular value $T_\lambda(\phi)$ from above. The curve $T = T_\lambda(\phi)$, defined by the condition $\mathcal{E}(k_\lambda; \phi, T) = 1/S(k_\lambda; \phi, T) = 0$, is referred to as the λ line [for the isochore of the figure, $T_\lambda(\phi = 0.15) = 0.6733$]. Taking the inverse FT of $[S(k) - 1]/n$ yields the total correlation function $h(r)$, and in Fig. 1(b), we plot the same information of Fig. 1(a) but in terms of the radial distribution function $g(r) = 1 + h(r)$. The results in this figure exhibit a notorious structural feature as T approaches $T_\lambda(\phi)$ from above, namely, the emergence of a long-range minimum in $g(r; \phi, T)$ at $r = r_{min}$ ($\approx 6\sigma$ in the RDF corresponding to the deepest quench, $T = 0.68$, in the figure). As we shall see later, this structural feature is an essential fingerprint of the process of cluster formation and eventual dynamic arrest due to cluster–cluster repulsions. Finally, note that Figs. 1(a) and 1(b) report the same information as Figs. 1 and 2 of Ref. 17 although at a different value of the parameter A (0.5 here and 0.082 in Ref. 17).

At this point, it is pertinent to clarify that the appearance of a low- k peak in the SF is a characteristic hallmark of many SALR systems (whether type I, II, and III), and it is generally associated with the emergence of additional ordering at a length scale much larger than the particle diameter σ . As discussed in Ref. 5, particularly referring to lysozyme protein solutions, this low- k peak is not necessarily related to the formation of clusters with optimal sizes and, hence, should more appropriately be referred to as an *intermediate range order* (IRO) peak.⁵ Notwithstanding this clarification, we can say, following the discussion of Refs. 17 and 27, that in our present type III SALR model system, it is safe to refer to $S(k_\lambda; \phi, T)$ as a “cluster” peak.

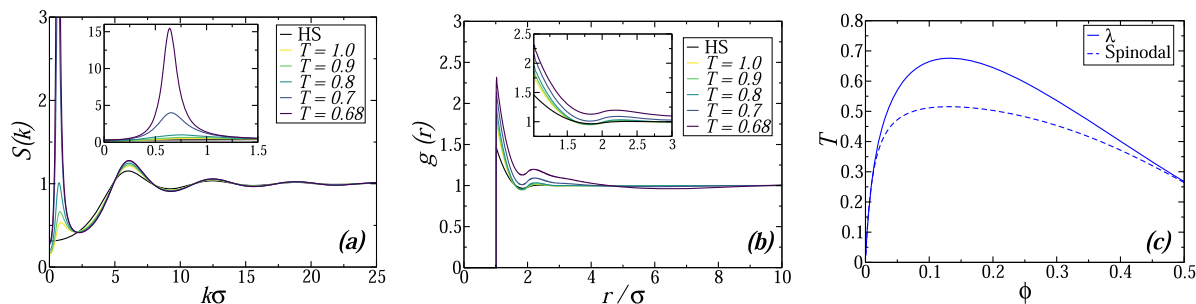


FIG. 1. Behavior of (a) the SF $S(k; n, T) = 1/n\mathcal{E}(k; n, T)$ and (b) the corresponding RDF $g(r; \phi, T)$, as provided by the RPA [Eq. (14)] for the HSDY fluid, with parameters $z_1 = 1$, $z_2 = 0.5$, and $A = 0.5$, for fixed volume fraction $\phi = 0.15$ and final temperatures above the λ line, $T > T_\lambda(\phi) = 0.6733$, as indicated. (c) Equilibrium gas–liquid phase diagram of the same HSDY fluid, exhibiting the spinodal (dashed line) and the λ (solid line) curves.

F. Equilibrium phase diagram of the HSDY model

The λ line $T_\lambda(\phi)$ of the system described in Figs. 1(a) and 1(b) is represented in Fig. 1(c). For reference, the spinodal line is also plotted and it was calculated from the approximate function $\mathcal{E}(k; n, T)$ in Eq. (14). This figure, which is our version of Fig. 6 of Ref. 17, summarizes the equilibrium phase diagram of the HSDY model predicted by the RPA, which indicates that the gas–liquid transition is preempted by the occurrence of the singular λ line, below which uniform disordered equilibrium states do not exist, since $S(k; \phi, T) = 1/n\mathcal{E}(k; \phi, T)$ is negative (and hence, non-physical) for wavevectors in an interval around k_λ .

With the aim of understanding this puzzling feature of the equilibrium phase behavior of the type III HSDY model, Archer and Wilding²⁷ carried out Monte Carlo simulations, showing that, under some circumstances, the repulsive part of the pair potential could lead to the replacement of the liquid–vapor coexistence by two first-order phase transitions. The first involves the coexistence of the vapor with a fluid of spherical liquid-like clusters, and the second involves the coexistence of a phase of spherical voids with the homogeneous liquid. These two transition lines meet with the vapor–liquid transition at a triple point. Later on, using density-functional theory, Archer *et al.*¹⁸ concluded that below the λ line, the equilibrium states consisted of non-uniform spatially ordered (or “modulated”) phases (see Fig. 5 of Ref. 18), thus theoretically supporting, in part, the equilibrium scenario advanced by Monte Carlo calculations.

III. GLASS TRANSITION DIAGRAMS

Unfortunately, careful experimental work in colloidal systems with competing interactions does not report the observation of these equilibrium ordered structures.^{39–44} Instead, as also suggested by extensive molecular dynamics simulations,^{33–35} what seems to surround or substitute the predicted spatially ordered phases are equilibrium fluids of finite-sized clusters and percolating gel-like states. So far, the experimental elusiveness in observing the aforementioned modulated phases in SALR systems remains unresolved. One possible reason, of course, is the fact such phases are theoretically predicted for type III SALR liquids while—according to Ref. 4—most model experimental SALR systems studied are of type I. A second possibility, however, is related to the fact that the cluster fluid and percolated gel-like states are able to evolve into genuinely arrested non-equilibrium states, whose nature is controlled by the interplay between repulsions and attractions and whose fundamental understanding poses even more complex technical and fundamental challenges.

The theoretical description of such dynamically arrested states, in fact, is typically out of the scope of conventional equilibrium theories and simulations and, hence, must be described from a genuinely non-equilibrium perspective, such as that provided by the solution of the NE-SCGLE Eqs. (2)–(6). In analyzing the solution of this set of equations, it is instructive to start by discussing their asymptotic long-time stationary limits. For this, we can consider two strategies: either we first take the stationary limit of Eqs. (2)–(6) and then analyze its solutions or else we first formally determine the full time-dependent solution of Eqs. (2)–(6) and then take the long-time stationary limit. Let us describe the results of these two strategies.

A. MCT-like “glass transition” diagram

The first strategy only considers stationary solutions that correspond to thermodynamic equilibrium states and only requires the knowledge of the thermodynamic function $\mathcal{E}(k; n, T)$. Its main result is the MCT-like “glass transition” diagram of the system,^{71,88} which determines the borderline of the region of the state space where no kinetic barriers will impede the system from reaching thermodynamic equilibrium.

To explain the concept of *glass transition diagram* (GTD), let us note that Eqs. (2)–(6) contain the description of the dynamic properties of *equilibrium fluids* as the particular limit in which the solution $S(k; t)$ of Eq. (2) has reached its equilibrium limit $S(k; t \rightarrow \infty) = S(k; n, T) = 1/n\mathcal{E}(k; n, T)$. In this limit, one recovers the original *equilibrium* SCGLE theory of dynamical arrest^{56–58} that describes the dynamics of *equilibrium fluids*. The corresponding SCGLE equations follow from replacing $S(k; t)$, $\Delta\zeta^*(\tau; t)$, $F(k, \tau; t)$, and $F_S(k, \tau; t)$ in Eqs. (4)–(6) by, respectively, $S(k)$, $\Delta\zeta^{*eq}(\tau) \equiv \Delta\zeta^*(\tau; t \rightarrow \infty)$, $F^{eq}(k, \tau) \equiv F(k; \tau; t \rightarrow \infty)$, and $F_S^{eq}(k, \tau) \equiv F_S(k; \tau; t \rightarrow \infty)$. As in MCT, the SCGLE theory provides equations for the so-called non-ergodicity parameters, which are the long- τ asymptotic limits $f^{eq}(k) \equiv F^{eq}(k, \tau \rightarrow \infty)$ and $f_S^{eq}(k) \equiv F_S^{eq}(k, \tau \rightarrow \infty)$.

In the case of the SCGLE theory, $f^{eq}(k)$ and $f_S^{eq}(k)$ can be written in terms of the SF, $S(k; n, T)$, and the squared localization length $\gamma^{eq}(\phi, T)$ [Eqs. (9) and (10) of Ref. 53], the latter being solution of the equation

$$\frac{1}{\gamma^{eq}(\phi, T)} = \frac{1}{6\pi^2 n} \int_0^\infty dk k^4 [S(k; n, T) - 1]^2 \lambda^2(k) \times \frac{1}{[\lambda(k)S(k; n, T) + k^2 \gamma^{eq}(\phi, T)][\lambda(k) + k^2 \gamma^{eq}(\phi, T)]}. \quad (16)$$

The dynamic order parameter $\gamma^{eq}(\phi, T)$ diverges at equilibrium and has a finite value at non-ergodic states. Thus, it partitions the state space (ϕ, T) into its ergodic and non-ergodic regions, with the ideal glass transition line being the borderline between them. The monotonically increasing (red) solid line of Fig. 2(a) is such fluid–glass transition line $T = T_c(\phi)$ for our HSDY model, obtained within the RPA for $S(k; n, T)$ in Eqs. (9) and (14). This liquid–glass transition line originates at high-temperatures and high-densities at the well-known hard-sphere glass transition, occurring at $\phi_c \approx 0.58$. At lower T and ϕ , it meets the λ line at the state point $(\phi_b, T_b) = (0.365, 0.452)$.

Upon crossing this transition line from the ergodic domain [region I of Fig. 2(a)] to the non-ergodic domain (region II), the order parameter $\gamma^{eq}(\phi, T)$ changes discontinuously from its equilibrium infinite value to a finite non-equilibrium value, and this discontinuous behavior characterizes what is referred to (borrowing MCT language) as a “type B” glass transition. An alternative dynamic order parameter is the normalized equilibrium long-time self-diffusion coefficient $D_L(\phi, T)/D_0 = b^{eq}(\phi, T) = b(t \rightarrow \infty; \phi, T)$, also provided by the solution of the SCGLE equations. This dynamic state function is finite and positive in region I and vanishes in region II and along the ideal fluid–glass transition line $T = T_c(\phi)$. Its value is represented in Fig. 2(a) by a color code, with the darkest color corresponding to the arrested region II.

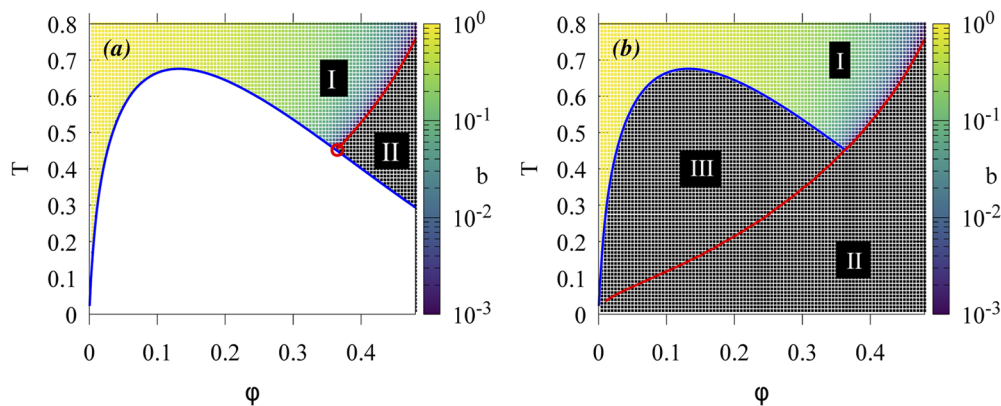


FIG. 2. (a) Glass transition diagram of the HSDY fluid with $z_1 = 1$, $z_2 = 0.5$, and $A = 0.5$, provided by the equilibrium SCGLE theory using Eq. (16). The blue solid line is the λ line and the red solid one is the fluid–glass transition line, with both meeting at the (“bifurcation”) point $(\phi_b, T_b) = (0.365, 0.452)$ (open circle). Region I identifies the ergodic region and region II identifies the glass region. The predicted equilibrium mobility at each state points (ϕ, T) is represented by a color code (colored region) above the λ line, with the black color representing the limiting condition $b^{eq}(\phi, T) = 0$. In the light empty region below the λ line, Eq. (16) cannot be used since $S(k; \phi, T)$ is non-physical. (b) Non-equilibrium glass transition diagram provided by the NE-SCGLE theory using Eq. (17). Above the λ line, it coincides with the glass transition diagram in (a) but adds the information that the λ line itself is a “type B” ergodic-to-non-ergodic transition line and that the fluid–glass transition line continues from above to below the λ line as a “type B” non-ergodic to non-ergodic transition line.

Clearly, since $S(k; n, T)$ does not exist below the λ line [non-monotonic (blue) solid line in Fig. 2(a)], the SCGLE theory cannot provide any predictions there. Thus, this method can identify the ergodic and non-ergodic regions only above the λ line, leaving the (light) region below, empty of information. This limitation is, of course, shared by MCT. In fact, our glass transition diagram in Fig. 2(a) is the analog of the MCT “kinetic phase diagrams” reported in Fig. 2 of Ref. 31 for different values of A , z_1 , and z_2 .

B. Non-equilibrium “glass transition” diagram (NEGTD)

The second strategy provides a route of escape from the limitation of the SCGLE theory to equilibrium conditions. For this, we must return to the full set of Eqs. (2)–(6) that summarize the more general NE-SCGLE formalism. Following the approach explained in detail in Ref. 68, one can extend the method based on the solution of Eq. (16) for $\gamma^{eq}(\phi, T)$ by introducing the more general parameter $\gamma^*(u)$, defined in Ref. 68 as the solution of its Eq. (3.6), namely,

$$\frac{1}{\gamma^*(u)} = \frac{1}{6\pi^2 n} \int_0^\infty dk k^4 [S^*(k; u) - 1]^2 \lambda^2(k; u) \times \frac{1}{[\lambda(k; u)S^*(k; u) + k^2 \gamma^*(u)][\lambda(k; u) + k^2 \gamma^*(u)]}, \quad (17)$$

where $S^*(k; u)$ is given by

$$S^*(k; u) \equiv [n\mathcal{E}(k; \phi, T)]^{-1} + \{S_i(k) - [n\mathcal{E}(k; \phi, T)]^{-1}\} e^{-2k^2 D_0 n \mathcal{E}(k; \phi, T) u}, \quad (18)$$

with $S_i(k) = S^*(k; u = 0)$ being an (arbitrary) initial condition.

For a given state point (ϕ, T) , we use $\mathcal{E}(k; \phi, T)$ to solve Eq. (17), which determines $\gamma^*(u)$ as a function of u . If we find that a finite value u_a of the parameter u exists, such that $\gamma^*(u)$ is infinite in the

finite interval $0 \leq u < u_a$ and finite for $u_a \leq u < \infty$, then we conclude that the system will become kinetically arrested. If, instead, $\gamma^*(u) = \infty$ for $0 \leq u < \infty$, we conclude that the state point (ϕ, T) lies in the ergodic region of state space. Thus, the functions $u_a(\phi, T)$ and $\gamma_a(\phi, T) \equiv \gamma^*(u_a(\phi, T))$ are dynamic order parameters, which allows us to draw what we refer to as the *non-equilibrium glass transition diagram* (NEGTD). In Fig. 2(b), we present the results corresponding to our specific HSDY model. Note that, contrary to the algorithm based on Eq. (16), whose input is the SF $S(k; n, T)$ (non-physical below the λ line), the input of this non-equilibrium algorithm is the thermodynamic stability function $\mathcal{E}(k; \phi, T)$, whose negative values simply indicate conditions of thermodynamic instability. As a result, this more general criterion to determine dynamic arrest is far more powerful than that based on Eq. (16), since it is also applicable to quenches to thermodynamically unstable regions of state space, as illustrated by the results in Fig. 2(b).

The NEGTD of Fig. 2(b) completely agrees with the GTD of Fig. 2(a), in that both algorithms partition the portion of the plane (ϕ, T) above the λ line into the two well-defined regions: region I of ergodic fluid states and region II of non-ergodic glass states. However, in the complementary portion of state space, i.e., at and below the λ line, the NE-SCGLE theory reveals a remarkable non-equilibrium scenario, whose first unexpected feature is the existence of two new dynamic arrest transitions for volume fractions below that of the meeting point (ϕ_b, T_b) . The first of them occurs at a dynamic arrest temperature that virtually coincides with the λ temperature $T_\lambda(\phi)$ and constitutes the boundary between the (ergodic) region I and a new region (region III) of dynamically arrested states, whose nature is expected to be revealed by their non-equilibrium structural and dynamical properties, provided by the full solution of the NE-SCGLE equations.

The second is a dynamic arrest transition occurring along the temperature $T = T_c(\phi) (< T_\lambda(\phi))$, which defines the boundary between the arrested states in region III and the glass states in the low-temperature–low-density extension of region II. These

two arrest lines merge at the meeting point (ϕ_b, T_b) , which is now revealed to actually be a point of bifurcation of the fluid-to-glass transition line of Fig. 2(a). The latter clearly appears to continue below the λ line (i.e., for $\phi \leq \phi_b$) as the arrested-glass transition line $T = T_c(\phi)$.

C. NE-SCGLE dynamic order parameter $\gamma_a^*(\phi, T)$

Most of the previous conclusions directly derive from the density and temperature dependence of the dynamic order parameters $u_a(\phi, T)$ and $\gamma_a(\phi, T)$, which, in turn, depend on (ϕ, T) through the function $\mathcal{E}(k; \phi, T)$ in Eq. (18). The parameter $\gamma_a(\phi, T)$ bears a more transparent physical significance, better explained by its original *equilibrium* definition: it is the long-time asymptotic value $\gamma^{eq} \equiv \lim_{\tau \rightarrow \infty} W^{eq}(\tau)$ of the mean squared displacement (MSD) $W^{eq}(\tau) \equiv \langle (\Delta \mathbf{r}(\tau))^2 / 3 \rangle^{eq}$ of individual particles. This parameter is infinite if the particles diffuse and is finite if they are immobilized, in which case it defines the square localization length. This definition extends to non-equilibrium conditions by explicitly including the waiting time t in the definition of the MSD, which is now defined as $W(\tau; t) \equiv \langle (\mathbf{r}(t + \tau) - \mathbf{r}(t))^2 / 3 \rangle$, thus allowing us to define the non-equilibrium square localization length γ_a as $\gamma_a \equiv \lim_{\tau \rightarrow \infty} \lim_{t \rightarrow \infty} W(\tau; t)$.

The use of the function $\gamma_a(\phi, T)$ is better illustrated in Fig. 3, which plots the inverse of $\gamma_a(\phi, T)$ as a function of the final temperature T along two isochores, $\phi = 0.15$ [Fig. 3(a)] and $\phi = 0.45$ [Fig. 3(b)]. In Fig. 3(a), the (red) dashed horizontal line on the right ($\gamma_a^{-1}(\phi, T) = 10^{-2}$) indicates, in reality, that the function $\gamma_a(\phi = 0.15, T)$ actually remains infinite for all final temperatures above a critical temperature of about 0.673 [which, within the resolution of the figure, coincides with the temperature of the λ line for that isochore, $T_\lambda(\phi = 0.15) = 0.6733$]. At this singular temperature, $\gamma_a(\phi, T)$ jumps *discontinuously* to a finite value $\gamma_a(\phi, T_\lambda^-) \approx 40$ (localization length $\sqrt{\gamma_a} \approx 6.3$), remaining finite for $T < T_\lambda(\phi)$. This implies that the λ line, besides being the threshold of the thermodynamic stability of uniform equilibrium states (leading to the conjectured equilibrium modulated phases below the λ line),

also seems to be an ergodic to non-ergodic transition line. In fact, since $\gamma_a(\phi, T)$ jumps discontinuously at $T = T_\lambda(\phi)$, it is a “type B” singularity (in MCT terminology).

Examining now temperatures below the λ line, we see that the parameter $\gamma_a(T)$ decreases continuously and exhibits a second discontinuity at a lower temperature $T_c(\phi = 0.15) = 0.165$. This discontinuity implies the existence of still a second dynamic arrest transition, now corresponding to a non-ergodic-to-non-ergodic (or “glass–glass”) “type B” transition, in which the dynamic order parameter $\gamma_a(T)$ changes discontinuously by about one order of magnitude, from a value $\gamma_a(T_c^+) \approx 4$ to another finite value $\gamma_a(T_c^-) \approx 0.025$ (localization length $\sqrt{\gamma_a} \approx 0.15$, typical of hard-sphere glasses). Besides these two discontinuities, we could not identify any other dynamically singular temperature. In fact, we found that the function $\gamma_a(\phi, T)$ is perfectly continuous through the spinodal curve $T = T_s(\phi)$, implying that this line of thermodynamic instability would be dynamically irrelevant if dynamical arrest were the only kinetic pathway available to the system.

Performing these calculations at other isochores allows us to determine the two glass transition lines [$T = T_\lambda(\phi)$ and $T = T_c(\phi)$] shown in Fig. 2(b), which merge at the bifurcation point (ϕ_b, T_b) into a single fluid–glass transition line and which coincides with that determined by the method of Subsection III A [see Fig. 2(a)]. For completeness, Fig. 3(b) illustrates the behavior of the function $\gamma_a(\phi = 0.45, T)$, corresponding to an isochore at the right of the bifurcation (ϕ_b, T_b) . In this case, one finds that $\gamma_a(\phi = 0.45, T)$ is infinite for temperatures above the fluid–glass transition line $T = T_c(\phi = 0.45) = 0.656$ and jumps discontinuously to a finite value $\gamma_a(\phi = 0.45, T_c^-) \approx 0.025$. To the right of the bifurcation ($\phi > \phi_b$), the function $\gamma_a(\phi, T)$ is continuous through both the λ line and the spinodal curve, implying that neither of these lines have any dynamical relevance in this regime ($\phi > \phi_b$).

Let us emphasize that the dynamic arrest scenario summarized by Fig. 2(b) appears at first sight to be essentially identical to that of the same model system in the absence of the repulsive Yukawa interaction (i.e., with $A = 0$; see Refs. 68–71). This is illustrated by comparing Fig. 2(b) with Fig. 4 of Ref. 68. There are, however,

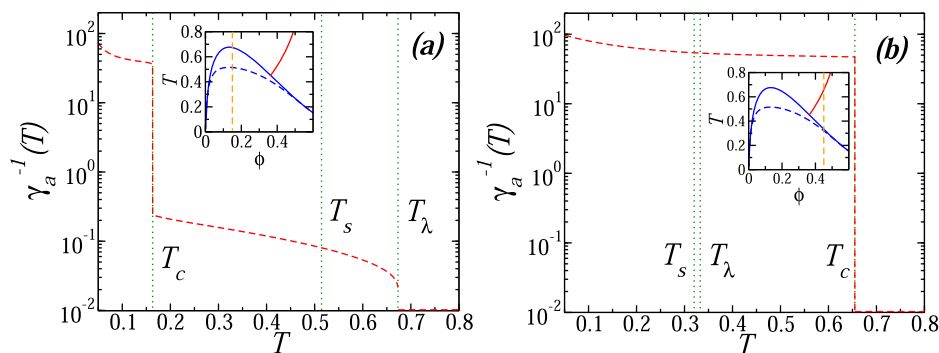


FIG. 3. Dependence of the non-equilibrium dynamic order parameter $\gamma_a(\phi, T)$ on the final temperature T for a sequence of quenches of the HSDY fluid ($z_1 = 1$, $z_2 = 0.5$, and $A = 0.5$) at fixed volume fraction ϕ and with initial condition $S_i(k) = S_{HS}^{eq}(k; \phi)$ for (a) $\phi = 0.15$ to the left of the bifurcation point $(\phi_b, T_b) = (0.365, 0.452)$ (see the vertical dashed line in the inset) and (b) $\phi = 0.45$ to the right of the bifurcation point. In (a), the vertical dotted lines indicate the three temperatures corresponding to the λ and spinodal lines and the glass-to-glass transition, thus highlighting the discontinuous jumps of γ_a at the two temperatures T_λ and T_c and also the fact that T_s passes completely unnoticed for the non-ergodicity parameter. In (b), the vertical lines emphasize that γ_a only jumps discontinuously at T_c and crosses the two lines of thermodynamic instabilities without noticing them.

remarkable fundamental differences. The most important of them is the nature of the dynamic arrest transition line $T = T_\lambda(\phi)$, along with the functions $u_a(\phi, T)$ and $\gamma_a(\phi, T)$, which jump from infinite values above the λ line to finite values below (type B transition). In the absence of the repulsive term, $A = 0$, there is no λ line, and the type B arrest line $T = T_\lambda(\phi)$ is replaced by an arrest line $T = T_s(\phi)$ lying along the spinodal curve. This transition happens to be of type A, i.e., the function $\gamma_a(\phi, T)$ passes continuously from infinite values above the line $T = T_s(\phi)$ to finite values below.

This qualitative difference between these two cases is, of course, associated with a remarkable *structural* difference between the arrested phases predicted immediately below each transition. Thus, in the absence of repulsions ($A = 0$), the NE-SCGLE theory predicts the formation, below $T = T_s(\phi)$, of spinodal-decomposition heterogeneities, whose growth is halted only by dynamic arrest mechanisms, as established and discussed in detail in Refs. 68 and 69. In contrast, in the presence of repulsions ($A > 0$), below $T = T_\lambda(\phi)$, the NE-SCGLE theory predicts the dynamic arrest due to the repulsion between finite-size clusters, as we now establish by analyzing the structural properties predicted by the NE-SCGLE theory.

IV. STATIONARY STRUCTURE FACTOR $S^a(k)$

Let us now discuss the structural properties of the HSDY model predicted by the NE-SCGLE theory, as described by the solution of Eq. (2) for $S(k; t)$. As carefully discussed in Ref. 68, the time-dependent NESF $S(k; t)$ is given by $S(k; t) = S^*(u(t))$, where the function $S^*(u)$ is defined in Eq. (18) and with the variable $u(t)$ being the “material” time $u(t) \equiv \int_0^t b(t') dt'$.⁶⁵ Before discussing the structural aging described by the full t -dependence of $S(k; t)$, however, it is useful to consider its stationary, long-time asymptotic limit $S^a(k) \equiv \lim_{t \rightarrow \infty} S(k; t)$, given by⁶⁸

$$S^a(k; \phi, T) \equiv [n\mathcal{E}(k; \phi, T)]^{-1} + \{S_i(k) - [n\mathcal{E}(k; \phi, T)]^{-1}\} \times e^{-2k^2 D_0 n \mathcal{E}(k; \phi, T) u_a(\phi, T)}, \quad (19)$$

with the initial condition $S_i(k)$ chosen here as the SF at infinite T , i.e., $S_i(k) = S(k; \phi, T = \infty) = S^{HS}(\phi)$.

Clearly, when the system is quenched to a state point (ϕ, T) in the ergodic region [infinite $u_a(\phi, T)$ and $\gamma_a(\phi, T)$], the system will equilibrate, and $S(k; t)$ will asymptotically attain its equilibrium value $S^a(k; \phi, T) = S(k; \phi, T)$. The salient features of $S(k; \phi, T)$ have been discussed thoroughly in the literature^{13,16,17} and were briefly illustrated in Fig. 1. The case of interest that the NE-SCGLE theory now allows us to discuss is, of course, when the state point (ϕ, T) lies in one of the non-ergodic regions [finite $u_a(\phi, T)$ and $\gamma_a(\phi, T)$], in which the system will no longer be able to equilibrate. Instead, $S(k; t)$ is expected to attain the non-equilibrium value $S^a(k; \phi, T)$ given by Eq. (19).

Figures 4 and 5 illustrate the dependence on the depth of the quench of both the NESF $S^a(k; \phi, T)$ and the corresponding NERDF $g^a(r; \phi, T) \equiv 1 + h^a(r; \phi, T)$, with the NETCF $h^a(r; \phi, T)$ being the inverse FT of $[S^a(k; \phi, T) - 1]/n$. To discuss the high-density–high-temperature scenario, Figs. 4(a) and 4(b) exhibit the behavior predicted for these structural properties along the isochore $\phi = 0.45$, which lies well to the right of the bifurcation point (ϕ_b, T_b) , as a function of T . In Fig. 4(a), we notice first the non-monotonic T -dependence of the hard-sphere-like correlations, represented by the height $S_{main}^a(\phi, T) \equiv S^a(k_{main}; \phi, T)$ of the main peak of $S^a(k; \phi, T)$, located at $k = k_{main} \approx 2\pi/\sigma$. As summarized in the inset of this figure, this property (described there by the solid line) first increases when T is decreased still in the ergodic regime, $T > T_c(\phi)$, but as T crosses the liquid–glass line, it decreases with smaller T . Note that the SF $S(k; \phi, T)$ still exists for $T \leq T_c(\phi)$ and the height $S(k_{main}; \phi, T)$ of its main peak continues to increase as T decreases below $T_c(\phi)$ (dashed line). The NE-SCGLE theory, however, predicts that below $T_c(\phi)$, this equilibrium $S(k; \phi, T)$ will be unreachable, in practice, due to kinetic considerations.³

Let us note also the qualitative resemblance of the non-equilibrium structure represented by $S^a(k; \phi, T)$ with the equilibrium structure of a fluid of particles with only excluded volume interactions. This is also observed in the dependence of the NERDF $g^a(r; \phi, T)$ illustrated in Fig. 4(b). To quantify this resemblance,

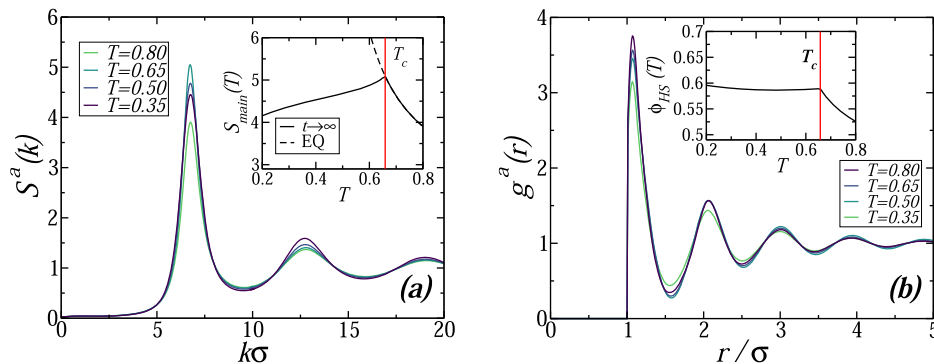


FIG. 4. Behavior of the stationary (a) NESF $S^a(k; \phi, T)$ and (b) NERDF $g^a(r; \phi, T)$ of the HSDY fluid ($z_1 = 1, z_2 = 0.5$ and $A = 0.5$), at fixed volume fraction $\phi = 0.45$ and for different (final) temperatures T above and below the liquid–glass transition $T_c(\phi = 0.45) = 0.656$, as indicated. The inset of (a) exhibits the T dependence of the height $S_{main}^a(\phi, T) \equiv S^a(k_{main}; \phi, T)$ of the main peak of $S^a(k; \phi, T)$ (darkest solid line) and of the equilibrium structure factor $S(k; \phi, T)$ (dashed line). The solid line in the inset of (b) represents the effective hard-sphere volume fractions $\phi_{HS}(\phi = 0.45, T)$, determined as described in the text.

let us borrow the notion of structural equivalence between equilibrium soft and hard-sphere fluids proposed in Refs. 89–91, and let us apply it to establish the structural equivalence between our non-equilibrium HSDY system and the equilibrium HS liquid. For this, we define an effective HS fluid whose RDF $g_{HS}(r; \phi_{HS})$ matches $g^a(r; \phi, T)$ at least in the height $g_2^a(\phi, T) \equiv g^a(r_2; \phi, T)$ of its second maximum, located at $r_2 \approx 2\sigma$.

This procedure assigns an effective HS volume fraction ϕ_{HS} to each state point (ϕ, T) . In the inset of Fig. 4(b), we plot the function $\phi_{HS} = \phi_{HS}(\phi, T)$ for $\phi = 0.45$, which reveals that in the ergodic region, $\phi_{HS}(\phi, T)$ increases with the depth of the quench until reaching a maximum similar in magnitude to the well-known hard-sphere glass transition volume fraction $\phi_c^{HS} = 0.58$ at $T \approx T_c$. Below the liquid–glass transition line $T = T_c(\phi)$, however, we observe that $\phi_{HS}(\phi, T)$ remains relatively constant, reminding the T -dependence of the inverse square localization length $\gamma_a^{-1}(\phi, T)$ below T_c [see Fig. 3(b)]. These results provide non-equilibrium evidences to conclude that when the fluid–glass transition is crossed along isochores in the high-density–high-temperature regime, to the right of the bifurcation point (ϕ_b, T_b) and far from the λ line, dynamical arrest is mainly driven by the excluded volume interactions and caging mechanisms. As a side observation, let us recall that the definition of the function $\phi_{HS} = \phi_{HS}(\phi, T)$ was based on the mapping of the non-equilibrium structure of the HSDY system onto the purely HS equilibrium structure. Such mapping is characteristic of the so-called “HS dynamic universality class.”^{90,91} This leaves open the provocative possibility that within adequate scalings, the asymptotic dynamics in this regime could also be mapped onto the equilibrium dynamics of the HS system.

We now move to the complementary (low-density–low-temperature) regime and consider the same isochore as in Fig. 1, $\phi = 0.15$, which lies well to the left of the bifurcation point. Going back to that figure, we recall that along this low-density isochore, the salient feature, amply discussed in the literature,^{7,13,16,17} was the emergence of the low- k (“cluster”) peak of the SF $S(k; \phi, T)$, centered at the wave vector denoted as k_λ . There, we learned that the height $S(k_\lambda; \phi, T)$ of this low- k peak increases monotonically

as the temperature is decreased until reaching the λ line, where it diverges. Figure 5(a) now complements this equilibrium story with its non-equilibrium continuation below the λ line, where the SF $S(k; \phi, T)$ ceases to exist, but the second, NESF $S^a(k; \phi, T)$ given by Eq. (19), emerges. This new non-equilibrium stationary solution represents, of course, the formation of amorphous dynamically arrested materials.

Figure 5(a) illustrates how $S^a(k; \phi, T)$ changes as the final temperature is lowered, now below $T_\lambda(\phi)$. The main trend observed is highlighted in the inset and refers to the notorious decrease with the quench depth of the height $S_\lambda^a(\phi, T) \equiv S^a(k_\lambda; \phi, T)$ of the low- k peak of $S^a(k; \phi, T)$, starting from its maximum value attained at $T \approx T_\lambda$ [e.g., $S_\lambda^a(\phi = 0.15, T = 0.67) \approx 500$] down to a value of ≈ 45 for T approaching the glass–glass transition $T_c = 0.165$ from above. Decreasing T below T_c , we observe that the height $S_\lambda^a(\phi = 0.15, T)$ of the small- k peak drops precipitously, down to values smaller than the height of the main (“particle–particle”) peak at $k \approx 2\pi/\sigma$. While this happens to the height $S_\lambda^a(\phi, T)$, we also observe a shift of the position k_λ of this peak, to larger wave-vectors, as T decreases below T_λ . This indicates that the size $\xi = 2\pi/k_\lambda$ of the corresponding spatial heterogeneities are largest at $T \approx T_\lambda$ (e.g., $\xi \approx 11\sigma$ at $T = 0.67$, slightly below T_λ) and decreases with the depth of the quench, down to approximately 6σ at $T = 0.17$ (slightly above T_c).

The same information is presented in Fig. 5(b) but in terms of the stationary NERDF $g^a(r; \phi, T)$. There, we see that the long-range minimum in the RDF $g(r; \phi, T)$ located at a distance $r_{\min} \approx 7\sigma$, recalling the lower temperature in Fig. 1(b) ($T = 0.68 > T_\lambda$), now continues to appear in the NERDF $g^a(r; \phi, T)$ for quenches below T_λ . This is illustrated by the shallowest quench of Fig. 5(b), with final temperature $T = 0.67$, whose NERDF $g^a(r; \phi, T)$ shows a much more pronounced long-range minimum at $r_{\min} \approx 7\sigma$ and a high long-range second maximum $g_2^a(\phi, T) \equiv g^a(r_\lambda; \phi, T)$ at $r_\lambda \approx 12\sigma$. These long-ranged minimum and maximum describe the cluster layering around a central particle (itself in a cluster). One notices, in addition, that the relevance of these features, measured by the heights $S^a(k_\lambda; \phi, T)$ or $g_2^a(r_\lambda; \phi, T)$, is largest

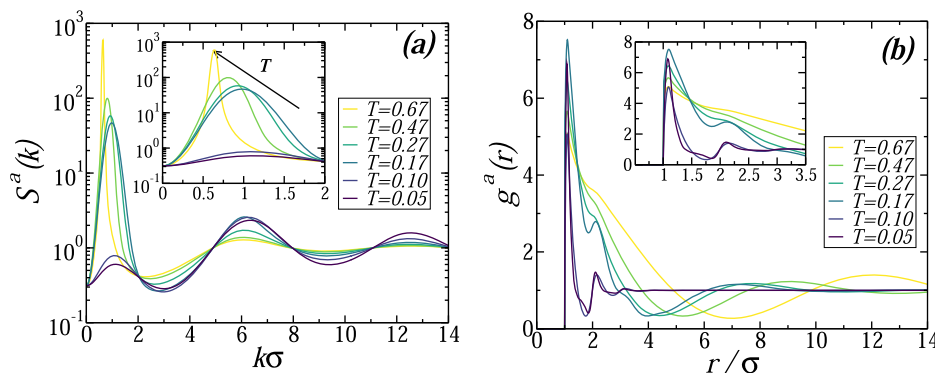


FIG. 5. Behavior of the stationary (a) NESF $S^a(k; \phi, T)$ and (b) NERDF $g^a(r; \phi, T)$ of the HSDY fluid ($z_1 = 1$, $z_2 = 0.5$, and $A = 0.5$), at fixed volume fraction $\phi = 0.15$ and for different temperature quenches below $T_\lambda(\phi = 0.15) = 0.6733$. The insets are auxiliary zooms to emphasize both the amplification of structural correlations around k_λ (or r_λ , according to the case) and the shift of k_λ (r_λ) toward smaller (larger) values with decreasing T . In both figures, one notices two qualitatively different behaviors: for shallow quenches, strong amplifications at low wave vector k_λ (or r_λ) and for deeper quenches, only a moderate amplification at $k \approx 2\pi/\sigma$.

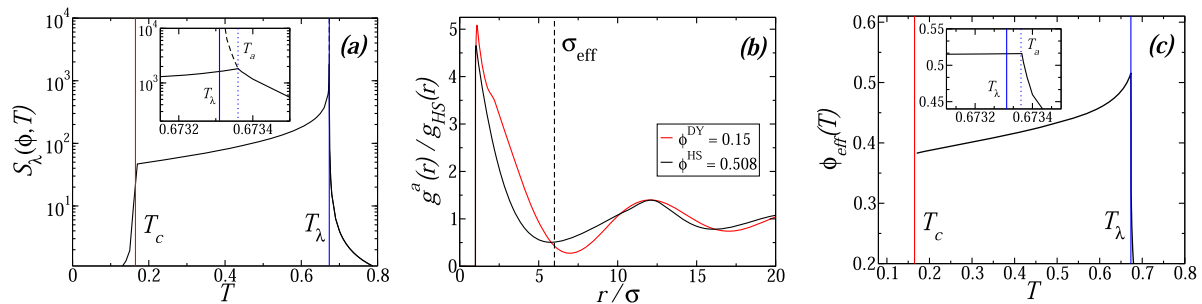


FIG. 6. (a) T -dependence of the height $S_\lambda^a(\phi, T) \equiv S^a(k = k_\lambda; \phi, T)$ of the NESF $S^a(k; \phi, T)$ along the isochore $\phi = 0.15$, covering temperatures from below the glass transition point T_c up to temperatures above the fluid–glass-transition temperature $T_a = 0.67336 > T_\lambda = 0.67331$ (see the text). The inset considers an amplification around T_a used to emphasize the deviations of $S_\lambda^a(\phi, T)$ (solid line) from the equilibrium value $S(k_\lambda; \phi; T)$ (dashed line), which diverges at T_λ . (b) Comparison of the behavior of the asymptotic value of the NERDF $g^a(r; \phi = 0.15, T = 0.67)$ (red solid line) and the effective hard-sphere RDF $g(r; \phi_{HS})$ (black solid line) used to match the height of the second maximum (see the text). (c) T -dependence of the volume fraction ϕ_{eff} of the effective hard-sphere fluid used to match the RDF for temperatures below the T_a transition line and slightly above the T_c transition (see the text).

in the neighborhood of the λ line and decreases with the quench depth.

To have a more comprehensive summary of these trends in the behavior of $S^a(k; \phi, T)$, in Fig. 6(a), we plot $S_\lambda^a(\phi = 0.15, T)$ as a function of T , covering temperatures from below the glass–glass transition temperature T_c up to temperatures above T_λ . There, we see that it is mostly in the temperature interval $T_c < T < T_\lambda$ where $S_\lambda^a(\phi, T)$ attains very large values, decreasing catastrophically outside this interval. Regarding the decay of $S_\lambda^a(\phi, T)$ with T in the close neighborhood of T_λ , if the dynamic arrest transition occurred exactly at T_λ , we should have a mathematical discontinuity right at T_λ , since $S_\lambda^a(\phi, T)$ remains finite as T approaches T_λ from below but diverges when T approaches T_λ from above.

A close inspection of such a singular prediction, however, revealed a rather unexpected scenario, illustrated in the inset of Fig. 6(a): as it turns out, the dynamic arrest transition does not occur at $T = T_\lambda$ but at a different, slightly larger temperature, which we denote T_a . More precisely, $T_\lambda = 0.67331$, whereas $T_a = 0.67336$ (clearly, to detect this difference we needed a very high numerical resolution). However, the consequence is that the dynamic arrest transition preempts the occurrence of the divergence of $S_\lambda^a(\phi, T)$, thus explaining the practical impossibility of its observation. Hence, although quantitatively modest, this observation may have far-reaching fundamental implications regarding the theoretical understanding of the accurate descriptions of cluster formation and dynamic arrest in SALR systems. In fact, although scanning the state space spanned by the potential parameters (z_1 , z_2 , and A) is out of the scope of the present work, let us mention that preliminary extensions of the present NE-SCGLE calculations reveal that the minute difference between T_λ and T_a becomes more significant when the range of the attraction decreases. We thus expect that a more detailed study in this direction will allow a more direct contact with the phenomenology of cluster formation revealed by simulations,^{33,36} performed for much narrower attractive wells than that discussed here. In this paper, however, we shall continue neglecting this quantitative difference between T_a and T_λ and will continue describing the dynamic arrest transition as occurring at the temperature T_λ .

On a different subject, let us now refer to the early and sharp analysis by Sciortino *et al.*,³³ who modeled the effective long-range cluster–cluster interaction as the superposition of the particle–particle Yukawa repulsion between the particles that form two interacting clusters. This led to a renormalized cluster–cluster Yukawa repulsion, capable of inducing dynamic arrest into a Wigner glass of clusters, very much as the experimentally observed^{32,93} Wigner glasses formed by individual charged colloidal particles. Along this line of thought, the long-range minimum and maximum of $g^a(r; \phi, T)$ in Fig. 5(b) should correspond to the first minimum and maximum of the RDF of a repulsive Yukawa fluid. However, since the repulsive Yukawa fluid is structurally equivalent to the hard-sphere fluid,^{90,91} we can also pursue this idea using the structural equivalence of the fluid of clusters with the hard sphere liquid.

This is best explained in Fig. 6(b), which compares the NERDF $g^a(r; \phi, T)$ (red solid line) corresponding to the shallowest quench in Fig. 5(b) (final temperature $T = 0.67$, slightly below $T_\lambda = 0.6733$), with the RDF $g(r; \phi_{HS})$ (black solid line) of an effective hard-sphere system that matches the height $g_\lambda^a(\phi, T) \equiv g^a(r_2; \phi, T)$ of the long-range second maximum at r_2 of $g^a(r; \phi, T)$. This comparison determines the HS volume fraction $\phi_{HS}(\phi, T)$ of an effective HS system structurally equivalent to the cluster–cluster correlations in the RDF $g^a(r; \phi, T)$ of the SALR system at the final state point (ϕ, T) . Figure 6(c) exhibits the value $\phi_{eff} \equiv \phi_{HS}(\phi = 0.15, T)$ thus computed, as a function of the final temperature T .

As observed in Fig. 6(c), ϕ_{eff} can be determined even in the equilibrium regime ($T > T_\lambda$) but only in the immediate neighborhood of T_λ , where it has a sharp increase as T approaches T_λ from above and where it reaches its maximum value (slightly larger than 0.5). For $T < T_\lambda$, we have that ϕ_{eff} decreases with decreasing T , down to a value $\phi_{eff} \lesssim 0.45$ in the neighborhood of the glass–glass transition temperature T_c . Thus, in the interval $T_c < T < T_\lambda$, the quantitative value of ϕ_{eff} in Fig. 6(c) is clearly smaller than the HS glass transition volume fraction $\phi_c \approx 0.58$ and, hence, cannot account for the dynamic arrest condition. This means that the cluster–cluster caging mechanism contributes to the arrest, but it is

not sufficient. Hence, other mechanisms must come into play in this regime.

Those additional mechanisms are also suggested by the results for $g^a(r; \phi, T)$ in Fig. 5(b). There, we see that as T decreases sufficiently, the true hard-sphere interactions manifest themselves in the emergence of a local maximum in $g^a(r; \phi, T)$ at $r \approx 2$, indicating growing particle-particle (not cluster-cluster) hard-sphere correlations. As the results in Fig. 5(b) indicate, these become the dominant correlations for T below the glass-glass transition temperature T_c .

In summary, we can say that in contrast with the high-density regime illustrated in Fig. 4, whose dynamic arrest was strongly dominated by the excluded volume forces, in the low-density-low-temperature regime, illustrated by the isochore $\phi = 0.15$, the dynamic arrest is the result of a much subtler and complex interplay between the three components of the interaction: the excluded volume, the long-range repulsion, and the shorter-ranged attraction.

V. STRUCTURAL AGING: t -DEPENDENCE OF $S(k; t)$ AND $g(r; t)$

At this point, it is important to emphasize that the equilibrium structure factor and phase diagram of Fig. 1, as well as the glass transition diagrams of Fig. 2 and the structural properties $S^a(k; \phi, T)$ and $g^a(r; \phi, T)$ just discussed, only refer to the infinitely long time asymptotic limit, whose experimental observability is only possible, in practice, if we wait longer than the longest relaxation times of the system. This may be almost trivial when the system is able to relax to equilibrium, which obviously makes the asymptotic equilibrium scenario verifiable within practical waiting times (and hence, much more familiar and representative of ordinary experience). Under conditions of dynamical arrest, however, the longest relaxation times may actually be too long (ideally, infinite), and the system might then remain in non-equilibrium conditions within any practical observation time. This, in turn, may render the asymptotic glass transition scenario impossible to verify in practice.

This practical impossibility could impede us to appreciate the value of these asymptotic predictions. Such impediment, however, can be removed by considering the full t -dependent solutions of the NE-SCGLE Eqs. (2)–(6), which predict what one would measure at

the finite and practical waiting times t involved in any realistic experiment or simulation. From this kinetic perspective, the fundamental role of the ideal asymptotic scenario may be best appreciated, as we now illustrate with the aging of the structural properties. Of course, the full t -dependent solution also yields a wealth of information regarding, for example, the dynamic and rheological properties, thus providing a more powerful resource to understand the nature of the glassy phases described by the asymptotic glass transition scenario.

To illustrate the structural aging predicted for the HSDY system, Fig. 7(a) plots the snapshots of the NESF $S(k; t)$ as a function of k , for a sequence of representative values of the waiting time t , after its instantaneous quench to the final temperature $T = 0.67$ along the isochore $\phi = 0.15$. These results correspond to the shallowest quench illustrated in Fig. 5 and exhibit the gradual enhancement of the correlations, starting from the chosen initial state $S(k; t = 0; \phi, T) = S^{eq}(k; \phi, T = \infty) = S^{HS}(k; \phi)$ (black solid line) and ending at the asymptotic solution $S^a(k; \phi, T) = S(k; t = \infty; \phi, T)$ (red dashed line). They also illustrate the kinetic build-up of a rather fast, but very modest, increase around the main peak at $k = k_{main} \approx 2\pi/\sigma$ of $S(k; t)$, along with the appearance of the small- k peak at $k = k_\lambda \approx 1/\sigma$, which exhibits, in contrast, a slower but far more spectacular enhancement.

The main peak around k_{main} describes short-ranged correlations, of the order of one HS diameter, and implies rather fast processes of nearest neighbors moving close to each other in the initial stage of cluster formation. The small- k peak at k_λ describes, instead, longer-ranged correlations, of the order of six HS diameters, and its slower kinetics is associated with the build-up of cluster-cluster correlations, ultimately leading to dynamic arrest. This striking kinetic difference is visualized more precisely in the inset of the Fig. 7(a), which compares $S_{main}(t; \phi, T) \equiv S(k_{main}, t; \phi, T)$ with $S_\lambda(t; \phi, T) \equiv S(k_\lambda, t; \phi, T)$ for the same t sequence.

Let us stress again that the information provided by the full t -dependent solutions of the NE-SCGLE Eqs. (2)–(6) is too abundant to be reviewed in one individual report, even if we restricted ourselves only to one specific property, such as to $S(k, t; \phi, T)$. The main reason is that this function depends on its four arguments, $(k, t; \phi, T)$, and it is not a simple task to scan this four-dimensional parameter space. Still, partial views of this dependence are particularly instructive. For example, Fig. 6(a) plotted $S(k, t; \phi, T)$ as a

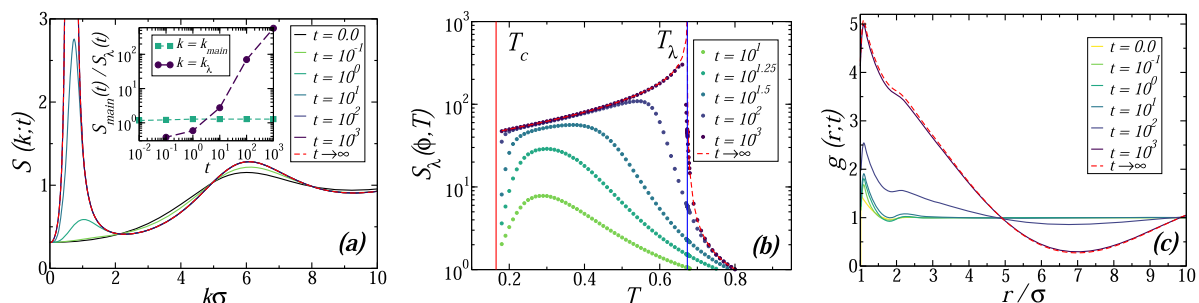


FIG. 7. (a) Sequence of snapshots describing the t -evolution of the NESF $S(k; t)$ for a quench of the HSDY system, at $\phi = 0.15$, from the same initial value as before and toward the final temperature $T = 0.67$ [right below $T_\lambda(\phi = 0.15)$]. The inset compares the time evolution of the two peaks $S_{main}(t)$ (solid squares) and $S_\lambda(t)$ (solid circles). (b) T -dependence of S_λ for a sequence of values of waiting times t , as indicated, along with the asymptotic long time value $S_\lambda(t \rightarrow \infty)$, also shown in Fig. 6(a). (c) Corresponding sequence of snapshots for the NERDF $g(r; t)$ (ϕ, T), along with the asymptotic value $g(r)^a(\phi, T)$.

function of T , keeping the other three arguments fixed, namely, $t = \infty$, $k = k_\lambda$, and $\phi = 0.15$. Since we now are analyzing the dependence of $S(k, t; \phi, T)$ on the waiting time t , we may now extend such analysis to finite t . This is done in Fig. 7(b), which plots $S_\lambda(t; \phi, T)$ for fixed $\phi = 0.15$, as a function of T for a sequence of values of the waiting time t .

The main message of Fig. 7(b) is that the NE-SCGLE theory not only predicts the results for $S_\lambda(t = \infty; \phi, T) = S_\lambda^a(\phi, T)$, which one would measure in an idealized and impossible experiment. A far more relevant practical prediction refers to what one should measure at the *finite* waiting times involved in real specific experiments or simulations. For instance, Fig. 7(b) illustrates the transient buildup of the structural correlations at k_λ , from which we learn that although this is a slow process compared with the buildup of the correlations at k_{main} , it only takes a finite time, $t \approx 10^3$, for $S(k_\lambda, t; \phi, T)$ to saturate to its asymptotic value $S_\lambda^a(t; \phi, T)$ within the resolution of the figure. Hence, the temptation to identify this process with one of equilibration is enormous. Fortunately, the corresponding analysis of dynamic properties, such as the α -relaxation time (not discussed in this paper), allows us to clearly discriminate between equilibration and arrest processes. Let us also mention a similarly interesting transient process, whose description can be drawn from Fig. 7(a). We refer to the fact that k_λ becomes increasingly smaller with t , thus describing the (time-dependent) cluster growth process.

The same structural information that we have just discussed can also be cast in terms of the NERDF $g(r, t; \phi, T)$. Here, we shall not make any effort to review the resulting scenario but only discuss Fig. 7(c), which is the real space counterpart of Fig. 7(a). This figure describes the aging of $g(r, t; \phi, T)$ (along $\phi = 0.15$), whose most relevant feature is the slow emergence of the long-ranged correlations associated with cluster-cluster correlations, the main mechanism for dynamic arrest in the shallow quench considered. From the aging of $g(r, t; \phi, T)$, the non-equilibrium evolution of other relevant structural quantities (such as coordination numbers, effective cluster size, and volume fraction) could be derived, each of which adds a distinct perspective to the general scenario of cluster formation and dynamic arrest. As said above, however, in our present contribution, we only aimed to pave the way to a more systematic discussion of both structural and dynamical properties. Such discussion is left for future work.

VI. DISCUSSION AND CONCLUSIONS

In summary, in this paper, we have carried out the first systematic application of the non-equilibrium self-consistent generalized Langevin equation (NE-SCGLE) theory to the description of dynamic arrest in liquids with competing short-ranged attractions and long-ranged repulsions (SALR). For this, we have analyzed the non-equilibrium structural behavior in a model hard-sphere plus double Yukawa (HSDY) fluid, quenched into its region of thermodynamical instability.

For clarity, we have restricted ourselves to the study of the non-equilibrium structural evolution of the model type III SALR after a quench into the regions of thermodynamical instability. The most fundamental quantity to understand such evolution is the thermodynamic stability function $\mathcal{E}(k; n, T)$. When interpreted as a familiar thermodynamic state function, it allows us to determine stability conditions, unstable domains, and equilibrium structural properties.

Its appearance in the kinetic Eq. (2), however, implies that $\mathcal{E}(k; n, T)$ bears a much deeper significance in determining more general non-equilibrium properties, such as the time-evolving structure factor $S(k; t)$. In this context, $\mathcal{E}(k; n, T)$ no longer represents only an equilibrium property. Instead, it becomes a fundamental input that determines the kinetics of the time-dependent structural correlations $S(k; t)$ and $g(r; t)$ (and of any other related property, such as those describing the non-equilibrium dynamics). In this sense, Eq. (2) can be viewed as an innovative proposal to extend the Ornstein Zernike equation to non-equilibrium conditions.

Restricted to the very specific set of parameters chosen in this study to represent the type III SALR interactions ($z_1 = 1$, $z_2 = 0.5$ and $A = 0.5$), the physical scenario predicted by the NE-SCGLE equations reveals a stunning and complex interplay between the thermodynamic instability represented by the so-called λ line $T = T_\lambda(\phi)$ and different underlying mechanisms for dynamical arrest. This interplay materializes in three distinct types of non-ergodic discontinuous (“type B”) transitions: (i) a “fluid to arrested-cluster” (F-AC) transition, occurring for concentrations below a threshold value $\phi_b = 0.365$ and moderately low temperatures, which, in practice, coincides with the λ line $T = T_\lambda(\phi)$; (ii) an “arrested-clusters to glass” (AC-G) transition $T = T_c(\phi)$, occurring in the same ϕ -regime but at lower temperatures; and (iii) a “fluid to glass” (F-G) hard-sphere-like transition, observed for $\phi > \phi_b$, also denoted as $T = T_c(\phi)$, to emphasize its smooth continuation inside the region of thermodynamic instability, as the previous AC-G transition [see Fig. 2(b)].

This asymptotic dynamic arrest transition scenario was greatly enriched by the discussion of the non-equilibrium structural properties represented by $S(k, t; \phi, T)$ and $g(r, t; \phi, T)$. We first discussed the asymptotic stationary limits $S^a(k; \phi, T)$ and $g^a(r; \phi, T)$, and then considered the non-equilibrium transient, provided by the full t -dependent solutions of the NE-SCGLE equations [Eqs. (2)–(6)]. Besides describing in some detail the most salient features, we also highlighted some seemingly innocuous observations. The most relevant of them refers to the fact that at first glance and for the specific HSDY model liquid considered in this work, the locus of the F-AC transition coincides, “in practice”, with the λ line $T = T_\lambda(\phi)$. These quotation marks needed a clarification, which was provided by the zoom in the inset of Fig. 6(a): a closer inspection with the lens of the NE-SCGLE theory revealed that, in fact, the F-AC transition occurs not exactly at the λ temperature but also at a dynamic arrest temperature $T_{(F-AC)}$ slightly higher, $T_{(F-AC)}(\phi) > T_\lambda(\phi)$. This immediately implied that the F-AC transition preempts the λ -instability, thus avoiding the divergence of the equilibrium structure factor expected to occur at the λ line. As a consequence, when the model SALR system is quenched right below T_λ , the dynamical arrest conditions may prevent it from reaching full equilibrium conditions.

This observation suggests the impossibility to experimentally observe the ordered inhomogeneous (“modulated”) equilibrium phases predicted for the type III SALR systems in the region of thermodynamic instability. As just explained, the development of these phases is expected to become interrupted by non-equilibrium dynamical arrest barriers. Unfortunately, to the best of our knowledge, no experimental results exist that can confirm (or disregard) these important predictions. Thus, our work could be a guide for future experiments on type III SALR systems, carried out to test the predicted non-equilibrium scenario just outlined. Similarly, the

existing experimental data for type I and II SALR liquids surely will serve as a motivation for further characterizations within the theoretical framework provided by the NE-SCGLE. We leave such tasks for further work.

The present work was not aimed at scanning the parameter space (z_1, z_2, A) of the HSDY potential, that is, to explore the physical scenario for type I and type II SALR systems. Instead, it was meant to pave the way to develop further systematic investigations with that and other purposes. An important pending issue refers to the fact that within the NE-SCGLE description of arrested states, the specific evolution of the structural correlations is intimately related, via Eq. (2), to the aging of the dynamics, with the former being represented in (2) by the mobility function $b(t)$. Since the specific kinetics of $S(k; t)$ determines the non-equilibrium relaxation of the dynamics, it is a pending task to characterize the aging of the dynamics along each of the transitions outlined in this work and to establish its connection to the non-equilibrium structural behavior discussed here. From previous work on attractive systems (i.e., in the absence of the long-ranged Yukawa repulsion), we anticipate an intricate dynamic landscape, originated in the complex interplay between thermodynamic instabilities and dynamical arrest, leading to distinct relaxation laws for the dynamics approaching each transition. All these aspects, however, shall be addressed in future work.

ACKNOWLEDGMENTS

This work was supported by the Consejo Nacional de Ciencia y Tecnología (CONACYT, México) through Postdoctoral Fellowship Grant No. I1200/224/2021 (L.F.E.-A.) and through Grant Nos. 320983, CB A1-S-22362, and LANIMFE 314881. The authors acknowledge the anonymous referees for their encouraging and constructive criticisms.

AUTHOR DECLARATIONS

Conflict of Interest

The authors have no conflicts to disclose.

Author Contributions

Ana Gabriela Carretas-Talamante: Conceptualization (equal); Data curation (equal); Formal analysis (equal); Investigation (equal); Validation (equal); Writing – review & editing (equal). **Jesús Benigno Zepeda-López:** Conceptualization (equal); Data curation (equal); Formal analysis (equal); Investigation (equal); Software (equal); Supervision (equal); Writing – review & editing (equal). **Edilio Lázaro-Lázaro:** Data curation (equal); Formal analysis (equal); Investigation (equal); Supervision (equal). **Luis Fernando Elizondo-Aguilera:** Conceptualization (equal); Formal analysis (equal); Investigation (equal); Writing – original draft (equal); Writing – review & editing (equal). **Magdaleno Medina-Noyola:** Conceptualization (equal); Formal analysis (equal); Funding acquisition (equal); Investigation (equal); Methodology (equal); Supervision (equal); Writing – original draft (equal); Writing – review & editing (equal).

DATA AVAILABILITY

The data that support the findings of this study are available from the corresponding author upon reasonable request.

REFERENCES

- ¹P. E. Ramírez-González and M. Medina-Noyola, *Phys. Rev. E* **82**, 061503 (2010).
- ²P. E. Ramírez-González and M. Medina-Noyola, *Phys. Rev. E* **82**, 061504 (2010).
- ³L. E. Sánchez-Díaz, P. E. Ramírez-González, and M. Medina-Noyola, *Phys. Rev. E* **87**, 052306 (2013).
- ⁴Y. Liu and Y. Xi, *Curr. Opin. Colloid Interface Sci.* **39**, 123 (2019).
- ⁵Y. Liu, L. Porcar, J. Chen, W.-R. Chen, P. Falus, A. Faraone, E. Fratini, K. Hong, and P. Baglioni, *J. Phys. Chem. B* **115**, 7238–7247 (2011).
- ⁶Y. Zhuang and P. Charbonneau, *J. Phys. Chem. B* **120**, 6178 (2016).
- ⁷J. Ruiz-Franco and E. Zaccarelli, *Annu. Rev. Condens. Matter Phys.* **12**, 51 (2021).
- ⁸J. D. van der Waals, *On the Continuity of the Gaseous and Liquid States*, Studies in Statistical Mechanics XIV, edited by J. S. Rowlinson (North-Holland, 1988).
- ⁹B. Widom, *Physica A* **263**, 500 (1999).
- ¹⁰E. J. W. Verwey and J. T. G. Overbeek, *Theory of the Stability of Lyophobic Colloids* (Elsevier, Amsterdam, 1948).
- ¹¹B. Derjaguin, *Kolloid-Z.* **69**, 155 (1934); *Acta Physicochim. URSS* **10**, 333 (1939); B. Derjaguin and L. Landau, *ibid.* **14**, 633 (1941).
- ¹²S. Asakura and F. Oosawa, *J. Polym. Sci.* **33**, 183 (1958).
- ¹³R. P. Sear and W. M. Gelbart, *J. Chem. Phys.* **110**, 4582 (1999).
- ¹⁴D. Pini, G. Jialin, A. Parola, and L. Reatto, *Chem. Phys. Lett.* **327**, 209 (2000).
- ¹⁵A. Imperio and L. Reatto, *J. Phys.: Condens. Matter* **16**, S3769 (2004).
- ¹⁶Y. Liu, W.-R. Chen, and S.-H. Chen, *J. Chem. Phys.* **122**, 044507 (2005).
- ¹⁷A. J. Archer, D. Pini, R. Evans, and L. Reatto, *J. Chem. Phys.* **126**, 014104 (2007).
- ¹⁸A. J. Archer, C. Ionescu, D. Pini, and L. Reatto, *J. Phys.: Condens. Matter* **20**, 415106 (2008).
- ¹⁹A. J. Archer, *Phys. Rev. E* **78**, 031402 (2008).
- ²⁰B. Chacko, C. Chalmers, and A. J. Archer, *J. Chem. Phys.* **143**, 244904 (2015).
- ²¹J. Schmalian and P. G. Wolynes, *Phys. Rev. Lett.* **85**, 836 (2000).
- ²²M. Tarzia and A. Coniglio, *Phys. Rev. Lett.* **96**, 075702 (2006).
- ²³M. Tarzia and A. Coniglio, *Phys. Rev. E* **75**, 011410 (2007).
- ²⁴Y. Zhuang, K. Zhang, and P. Charbonneau, *Phys. Rev. Lett.* **116**, 098301 (2016).
- ²⁵A. de Candia, E. DelGado, A. Fierro, N. Sator, M. Tarzia, and A. Coniglio, *Phys. Rev. E* **74**, 010403(R) (2006).
- ²⁶A. Imperio and L. Reatto, *J. Chem. Phys.* **124**, 164712 (2006).
- ²⁷A. J. Archer and N. B. Wilding, *Phys. Rev. E* **76**, 031501 (2007).
- ²⁸P. D. Godfrin, N. E. Valadez-Pérez, R. Castañeda-Priego, N. J. Wagner, and Y. Liu, *Soft Matter* **10**, 5061 (2014).
- ²⁹J. Groenewold and W. K. Kegel, *J. Phys. Chem. B* **105**, 11702 (2001).
- ³⁰J. Groenewold and W. K. Kegel, *J. Phys.: Condens. Matter* **16**, S4877 (2004).
- ³¹J. Wu, Y. Liu, W.-R. Chen, J. Cao, and S.-H. Chen, *Phys. Rev. E* **70**, 050401 (2004).
- ³²A. Coniglio, L. De Arcangelis, E. Del Gado, A. Fierro, and N. Sator, *J. Phys.: Condens. Matter* **16**, S4831 (2004).
- ³³F. Sciortino, S. Mossa, E. Zaccarelli, and P. Tartaglia, *Phys. Rev. Lett.* **93**, 055701 (2004).
- ³⁴S. Mossa, F. Sciortino, P. Tartaglia, and E. Zaccarelli, *Langmuir* **20**, 10756 (2004).
- ³⁵F. Sciortino, P. Tartaglia, and E. Zaccarelli, *J. Phys. Chem. B* **109**, 21942 (2005).
- ³⁶P. Charbonneau and D. R. Reichman, *Phys. Rev. E* **75**, 050401(R) (2007).
- ³⁷J. A. Bollinger and T. M. Truskett, *J. Chem. Phys.* **145**, 064902 (2016).
- ³⁸B. A. Lindquist, S. Dutta, R. B. Jadrich, D. J. Milliron, and T. M. Truskett, *Soft Matter* **13**, 1335 (2017).
- ³⁹H. Sedgwick, S. U. Egelhaaf, and W. C. K. Poon, *J. Phys.: Condens. Matter* **16**, S4913 (2004).
- ⁴⁰A. Stradner, H. Sedgwick, F. Cardinaux, W. C. K. Poon, S. U. Egelhaaf, and P. Schurtenberger, *Nature* **432**, 492 (2004).

- ⁴¹F. Bordi, C. Cametti, M. Diociaiuti, and S. Sennato, *Phys. Rev. E* **71**, 050401(R) (2005).
- ⁴²A. I. Campbell, V. J. Anderson, J. S. van Duijneveldt, and P. Bartlett, *Phys. Rev. Lett.* **94**, 208301 (2005).
- ⁴³C. J. Dibble, M. Kogan, and M. J. Solomon, *Phys. Rev. E* **74**, 041403 (2006).
- ⁴⁴C. L. Klix, C. P. Royall, and H. Tanaka, *Phys. Rev. Lett.* **104**, 165702 (2010).
- ⁴⁵M. Mézard and G. Parisi, *Phys. Rev. Lett.* **82**, 747 (1999).
- ⁴⁶M. Grousson, V. Krakoviack, G. Tarjus, and P. Viot, *Phys. Rev. E* **66**, 026126 (2002).
- ⁴⁷P. L. Geissler and D. R. Reichman, *Phys. Rev. E* **69**, 021501 (2004).
- ⁴⁸W. Götze, in *Liquids, Freezing and Glass Transition*, edited by J. P. Hansen, D. Levesque, and J. Zinn-Justin (North-Holland, Amsterdam, 1991).
- ⁴⁹W. Götze and L. Sjögren, *Rep. Prog. Phys.* **55**, 241 (1992).
- ⁵⁰L. Berthier and G. Biroli, *Rev. Mod. Phys.* **83**, 587 (2011).
- ⁵¹L. Yeomans-Reyna and M. Medina-Noyola, *Phys. Rev. E* **64**, 066114 (2001).
- ⁵²L. Yeomans-Reyna, H. Acuña-Campa, F. Guevara-Rodríguez, and M. Medina-Noyola, *Phys. Rev. E* **67**, 021108 (2003).
- ⁵³R. Juárez-Maldonado *et al.*, *Phys. Rev. E* **76**, 062502 (2007).
- ⁵⁴M. A. Chávez-Rojo and M. Medina-Noyola, *Physica A* **366**, 55 (2006).
- ⁵⁵M. A. Chávez-Rojo and M. Medina-Noyola, *Phys. Rev. E* **72**, 031107 (2005); **76**, 039902 (2007).
- ⁵⁶L. Yeomans-Reyna, M. A. Chávez-Rojo, P. E. Ramírez-González, R. Juárez-Maldonado, M. Chávez-Páez, and M. Medina-Noyola, *Phys. Rev. E* **76**, 041504 (2007).
- ⁵⁷R. Juárez-Maldonado and M. Medina-Noyola, *Phys. Rev. E* **77**, 051503 (2008).
- ⁵⁸L. E. Sánchez-Díaz, A. Vizcarra-Rendón, and R. Juárez-Maldonado, *Phys. Rev. Lett.* **103**, 035701 (2009).
- ⁵⁹L. F. Elizondo-Aguilera and Th. Voigtmann, *Phys. Rev. E* **100**, 042601 (2019).
- ⁶⁰P. E. Ramírez-González and M. Medina-Noyola, *J. Phys.: Condens. Matter* **21**, 504103 (2009).
- ⁶¹L. Onsager, *Phys. Rev.* **37**, 405 (1931).
- ⁶²L. Onsager, *Phys. Rev.* **38**, 2265 (1931).
- ⁶³L. Onsager and S. Machlup, *Phys. Rev.* **91**, 1505 (1953).
- ⁶⁴S. Machlup and L. Onsager, *Phys. Rev.* **91**, 1512 (1953).
- ⁶⁵R. Peredo-Ortiz, M. Medina-Noyola, T. Voigtmann, and L. F. Elizondo-Aguilera, *J. Chem. Phys.* **156**, 244506 (2022).
- ⁶⁶G. Pérez-Ángel, L. E. Sánchez-Díaz, P. E. Ramírez-González, R. Juárez-Maldonado, A. Vizcarra-Rendón, and M. Medina-Noyola, *Phys. Rev. E* **83**, 060501(R) (2011).
- ⁶⁷P. Mendoza-Méndez, E. Lázaro-Lázaro, L. E. Sánchez-Díaz, P. E. Ramírez-González, G. Pérez-Ángel, and M. Medina-Noyola, *Phys. Rev. E* **96**, 022608 (2017).
- ⁶⁸J. M. Olais-Govea, L. López-Flores, and M. Medina-Noyola, *J. Chem. Phys.* **143**, 174505 (2015).
- ⁶⁹J. M. Olais-Govea, L. López-Flores, and M. Medina-Noyola, *Phys. Rev. E* **98**, 040601(R) (2018).
- ⁷⁰J. M. Olais-Govea, L. López-Flores, J. B. Zepeda-López, and M. Medina-Noyola, *Sci. Rep.* **9**, 16445 (2019).
- ⁷¹J. B. Zepeda-López and M. Medina-Noyola, *J. Chem. Phys.* **154**, 174901 (2021).
- ⁷²L. E. Sánchez-Díaz, E. Lázaro-Lázaro, J. M. Olais-Govea, and M. Medina-Noyola, *J. Chem. Phys.* **140**, 234501 (2014).
- ⁷³T. Voigtmann, *Europhys. Lett.* **96**, 36006 (2011).
- ⁷⁴E. Lázaro-Lázaro *et al.*, *Phys. Rev. E* **99**, 042603 (2019).
- ⁷⁵P. E. Ramírez-González, L. E. Sánchez-Díaz, M. Medina-Noyola, and Y. Wang, *J. Chem. Phys.* **145**, 191101 (2016).
- ⁷⁶L. F. Elizondo-Aguilera, P. F. Zubieta-Rico, H. Ruíz Estrada, and O. Alarcón-Waess, *Phys. Rev. E* **90**, 052301 (2014).
- ⁷⁷E. C. Cortés-Morales, L. F. Elizondo-Aguilera, and M. Medina-Noyola, *J. Phys. Chem. B* **120**, 7975 (2016).
- ⁷⁸R. Peredo-Ortiz, P. F. Zubieta Rico, E. C. Cortés-Morales, G. G. Pérez-Ángel, T. Voigtmann, M. Medina-Noyola, and L. F. Elizondo-Aguilera, *J. Phys.: Condens. Matter* **34**, 084003 (2022).
- ⁷⁹L. F. Elizondo-Aguilera, E. C. Cortés-Morales, P. F. Zubieta Rico, M. Medina-Noyola, R. Castañeda-Priego, T. Voigtmann, and G. Pérez-Ángel, *Soft Matter* **16**, 170 (2020).
- ⁸⁰The short-time self-diffusion coefficient D^0 is related by Einstein's relation, $D^0 = k_B T / \zeta^0$, with ζ^0 being the corresponding short-time friction coefficient [determined by its Stokes expression⁸¹ in colloidal liquids or by the kinetic (or "Doppler"⁸²) friction coefficient in the case of molecular liquids⁸³].
- ⁸¹L. D. Landau and E. M. Lifshitz, *Fluid Mechanics* (Pergamon, New York, 1959).
- ⁸²G. E. Uhlenbeck and L. S. Ornstein, *Phys. Rev.* **36**, 823 (1930).
- ⁸³L. López-Flores, P. Mendoza-Méndez, L. E. Sánchez-Díaz, L. L. Yeomans-Reyna, A. Vizcarra-Rendón, G. Pérez-Ángel, M. Chávez-Páez, and M. Medina-Noyola, *Europhys. Lett.* **99**, 46001 (2012).
- ⁸⁴D. A. McQuarrie, *Statistical Mechanics* (Harper and Row, 1973).
- ⁸⁵R. Evans, *Adv. Phys.* **28**, 143 (1979).
- ⁸⁶J. K. Percus and G. J. Yevick, *Phys. Rev.* **110**, 1 (1957).
- ⁸⁷L. Verlet and J.-J. Weis, *Phys. Rev. A* **5**, 939 (1972).
- ⁸⁸M. Sperl, *Phys. Rev. E* **69**, 011401 (2004).
- ⁸⁹F. de J. Guevara-Rodríguez and M. Medina-Noyola, *Phys. Rev. E* **68**, 011405 (2003).
- ⁹⁰P. E. Ramírez-González, L. López-Flores, H. Acuña-Campa, and M. Medina-Noyola, *Phys. Rev. Lett.* **107**, 155701 (2011).
- ⁹¹L. López-Flores, H. Ruíz-Estrada, M. Chávez-Páez, and M. Medina-Noyola, *Phys. Rev. E* **88**, 042301 (2013).
- ⁹²H. M. Lindsay and P. M. Chaikin, *J. Chem. Phys.* **76**, 3774 (1982).
- ⁹³E. B. Sirota, H. D. Ou-Yang, S. K. Sinha, P. M. Chaikin, J. D. Axe, and Y. Fujii, *Phys. Rev. Lett.* **62**, 1524–1527 (1989).